VERTICAL AXIS HYDROKINETIC GORLOV TURBINE FOR LOW FLOW AND LOW HEAD CONDITIONS

_____

A Final Year Project Report

Presented to

SCHOOL OF MECHANICAL & MANUFACTURING ENGINEERING

Department of Mechanical Engineering

NUST

ISLAMABAD, PAKISTAN

_____

In Partial Fulfillment

Of the Requirements for the Degree of

Bachelors of Mechanical Engineering

_____

By

Syed Mazhar Abbas Naqvi

Saad Tahir

Zain Ahmed

May 2019

EXAMINATION COMMITTEE

We hereby recommend that the final year project report prepared under our supervision by:

SYED MAZHAR ABAS NAQVI	124895
SAAD TAHIR	120377
ZAIN AHMED	124505

Titled: "VERTICAL AXIS HYDROKINETIC GORLOV TURBINE FOR LOW FLOW AND LOW HEAD CONDITIONS" be accepted in partial fulfillment of the requirements for the award of BACHELORS OF MECHANICAL ENGINEERING degree with grade ___

Supervisor: Dr. Muhammad Sajid SMME, NUST	Dated:
Committee Member: Dr. Mian Ashfaq SMME, NUST	Dated:
Committee Member: Dr. Zaib Ali SMME, NUST	Dated:

_____ _____

(Head of Department) (Date)

COUNTERSIGNED

Dated: _____ _____

(Dean / Principal

ABSTRACT

Pakistan is a developing country that is currently facing severe power demand-supply gap due to high population, rapid urbanization and traditional means of power generation. The heavy dependence of power sector on imported fossil fuels enforces an unembellished burden on economy of Pakistan and poses threatening environmental concerns. This study aims to evaluate the technical feasibility of a Gorlov (Helical Type) Vertical Axis hydrokinetic turbine to be installed in low-pressure, low-head open flow channels, targeting the rivers and canals worldwide. The analytical foundation was based on Q-Blade simulations employing Double Multiple Stream Tubes (DMST) theory to propose a turbine design with optimum power generation and self-starting capabilities under design conditions.

The various parameters impacting turbine design include radius of the turbine, chord length, aspect ratio, solidity and blade wrap. Multiple designs were considered and a non-dimensionalized trend was obtained for turbine efficiency and self-starting capability at various aspect ratios with decreasing efficiencies for increasing solidity values thereby constituting a trade-off between aforementioned operating characteristics. A SolidWorks CAD package was used to develop a model for virtual analysis and construction. The results produced by analytical modeling were then verified by conducting a rigorous three-dimensional Computational Fluid Dynamics analysis under transient conditions. Standard initialization was used with calculated initial conditions to ensure maximum convergence rate.

The results show that the proposed 4-blade turbine with 0.38m height, 0.25m diameter, 100% blade wrap, NACA-0018 airfoil, 0.25 Coefficient of Performance, 0.29 solidity will produce up to 63 W power and 4.3 Nm torque at maximum flow speed of $2.7ms^{-1}$. The manufacturing will include 3D printing the blades to create the mold for casting. The wet operating conditions for various parts of the assembly were factored in the choice of materials.

ACKNOWLEDGEMENTS

First and foremost, we would like to thank Allah for the wisdom and vision he bestowed upon us and for blessing us with the will and courage to take upon this project. We would like to extend our utmost gratitude to our faculty advisor, **Dr. Muhammad Sajid**, who has shared with us his guidance, knowledge and precious time. Moreover, a big thank you is in the works for **Dr. Adeel Javed** and his students for helping us set-up our computer simulations.

We would also show our gratitude to our seniors **Ali Hamza** and **Farhan Rafique** for giving us the guidelines that we needed to jump start our project and in understanding of Micro Hydro Turbines. Last but not the least we would like to pay our regards to **Engineer Naveed Hassan** and **Mr. Faisal** who have provided us with invaluable insight regarding the physical set-up of our testing assembly

ORIGINALITY REPORT

We certify that this research work titled "**Vertical Axis Hydrokinetic Gorlov Turbine for Low Flow and Low Head Conditions***"* is our own work. The work has not been presented elsewhere for assessment. The material that has been used from other sources it has been properly acknowledged / referred. We have not copied anything or anyone else's work and the work done is original and all result of our own hard work.

Syed Mazhar Abbas Naqvi

00000124895

Saad Tahir

00000120377

Zain Ahmed

00000124505

COPYRIGHT

- Copyright in text of this thesis rests with the student author. Copies (by any process) either in full, or of extracts, may be only in accordance with the instructions given by author and lodged in the Library of SMME, NUST. Details may be obtained by the librarian. This page must be part of any such copies made. Further copies (by any process) of copies made in accordance with such instructions may not be made without the permission (in writing) of the author.

- The ownership of any intellectual property rights which may be described in this thesis is vested in SMME, NUST, subject to any prior agreement to the contrary, and may not be made available for use of third parties without the written permission of SMME, NUST which will describe the terms and conditions of any such agreement.

- Further information on the conditions under which disclosure and exploitation may take place is available from the library of SMME, NUST Islamabad.

CONTENTS

ABSTRACT iii

ACKNOWLEDGEMENTS iv

ORIGINALITY REPORT v

COPYRIGHT vi

LIST OF TABLES xi

LIST OF FIGURES xii

ABBREVIATIONS xiv

NOMENCLATURE xv

1. INTRODUCTION 17

1.1. MOTIVATION 17

1.1.1. Hydro Energy 19

1.2. PROBLEM STATEMENT 20

1.3. OBJECTIVES 20

2. LITERATURE REVIEW 21

2.1. HYDROKINETIC TURBINES 21

2.1.1. Advantages 21

2.1.2. Limitations 22

2.2. NEED FOR HYDROKINETIC TURBINES 23

2.3. TYPES OF TURBINES 23

2.3.1. Mechanism Used to Harness Flow Energy 23

2.3.2. Orientation of Turbine Relative to Flow 25

2.4. DESIGN SELECTION 28

2.4.1. Mechanism of Operation 28
2.4.2 Orientation of Turbine Relative to Flow 28
3. ANALYTICAL MODELING 29
3.1. BASICS OF TURBINE PERFORMANCE ANALYSIS 29
3.2. DOUBLE MULTIPLE STREAM MODEL 31
3.3. Q-BLADE 32
3.4. DESIGN PARAMETERS 33
3.4.1. Blade Profile 33
3.4.2. Number of Blades 36
3.4.3. Blade Wrap 37
3.4.4. Solidity 38
3.4.5. Aspect Ratio 39
3.5. CONCLUSION 40
4. CFD ANALYSIS 41
4.1. IMPORTANCE OF CFD ANALYSIS 41
4.2. CREATION OF GEOMETRY 41
4.3. MESH DEFINITION 42
4.4. SOLVER SELECTION 44
4.4.1. Solver Analysis 44
4.5. THE WALL FUNCTION APPROACH 45
4.6. FLUENT MODEL 46
4.7. RESIDUAL VALUES 47
4.8. GRID INDEPENDENCE 48

4.9. RESULTS AND DISCUSSION 49
4.10. CONCLUSION 51
5. MANUFACTURING OF TURBINE ASSEMBLY 52
5.1. DESIGN PARAMETERS 52
5.2. BLADES FABRICATION TECHNIQUE 53
5.2.1. 3D Printing 53
5.2.2. Machining 53
5.2.3. Sand 53
5.3. FASTENING TECHNIQUE 54
5.4. DETAILED MANUFACTURING PROCESURE 54
5.4.1. 3D Printing 54
5.4.2. Sand Casting 55
5.4.3. Buffing 56
5.4.4. Welding 56
5.4.5. Support Design 58
5.4.6. Balancing 58
6. INSTRUMENTATION DEVELOPMENT 59
6.1. NOVELTY: PERFORMANCE ANALYSIS METHODOLOGY 59
6.1.1. Incorporation of an Electrical System 59
6.1.2. Development of a Mechanical System 59
6.2. INSTRUMENTATION TIMELINE 60
6.2.1. Light Weight Pulleys 60
6.2.2. Tailored Rope 61

6.2.3. Strong Support 61
6.2.4. Force Meter 62
6.2.5. Weights 62
6.2.6. Bearing Selection 63
6.2.7. Shaft Design 63
6.2.8. Turbine Central Shaft Calculation 64
6.3. FINAL ASSEMBLY 68
7. RESULTS AND DISCUSSIONS 69
7.1. TEST SITE 69
7.2. PERFORMANCE CURVES 70
7.3. RESULTS VERIFICATION 72
7.4. ERROR ANALYSIS 72
8. CONCLUSION 75
8.1. FUTURE RECOMMENDATIONS 76
9. REFERENCES 77
APPENDIX 1: DATA ACQUISION 78
APPENDIX 2: MATLAB CODE FOR PERFORMANCE CURVES 80

LIST OF TABLES

Table 1-Design comparison [8] 27

Table 2-Final turbine parameters 40

Table 3-Final blade parameters 40

Table 4-Number of Elements, Nodes and Y-Function for corresponding Body Size 42

Table 5-Power and Coefficient of Performance calculation from moment values 49

Table 6-Result comparison: Analytical vs. CFD 51

Table 7-Material selection matrix 54

Table 8-Shaft parameters 64

Table 9-Shaft material properties 67

Table 10-Test Matrix for Experiment 1 79

Table 11-Test Matrix for Experiment 2 79

Table 12-Test Matrix for Experiment 3 79

Table 13-Test Matrix for Experiment 4 80

LIST OF FIGURES

Figure 1-World energy consumption by resource [5] 18
Figure 2-Classification of hydrokinetic turbines 25
Figure 3-Axial flow turbines [12] 26
Figure 4-Cross flow turbines [12] 26
Figure 5-Forces on an airfoil section [14] 29
Figure 6-Turbine blade based on NACA Airfoil 33
Figure 7-Airfoil profile comparison 34
Figure 8-NACA 0018 Airfoil in Q-Blade 35
Figure 9-Comparative Analysis of Profile Performance 35
Figure 10-Turbine model generated in Q-Blade 36
Figure 11-Effect of number of blades on turbine performance 37
Figure 12-Top view of turbine model 38
Figure 13-Non-Dimensionality Analysis 39
Figure 14-CAD Model 41
Figure 15-Mesh for Body Size: 5mm 42
Figure 16-Mesh for Body Size: 6mm 43
Figure 17-Mesh for Body Size: 7mm 43
Figure 18-Mesh for Body Size: 9mm 43
Figure 19-Domain model for CFD simulation 47
Figure 20-Residual Values for CFD Simulation 48
Figure 21-Pressure contour 50
Figure 22-Velocity vectors 50

Figure 23-Final Dimensions of Turbine 52
Figure 24-3D Printed Blade Pattern 55
Figure 25-Filing of Blades 55
Figure 26-Grinding and Buffing of Blades 56
Figure 27-Manufacturing Defects 57
Figure 28-Turbine Rotor 57
Figure 29-Support Collar 58
Figure 30-Static Balancing Assembly 58
Figure 31-Teflon Pulleys 60
Figure 32-Purpose-built Rope 61
Figure 33-Support for Rope Pulley Dynamometer Assembly 61
Figure 34-Digital Force Meter 62
Figure 35-Weights and Hanger 62
Figure 36-UCP 202 Bearing 63
Figure 37-Consolidated Forces and Moments on Shaft 66
Figure 38-Force Distribution on Shaft 67
Figure 39-Prototype Assembly 68
Figure 40-Turbine under operation (unloaded) 69
Figure 41-Turbine under operation (loaded) 69
Figure 42-Torque vs RPM Curve 71
Figure 43-Power vs RPM Curve 71
Figure 44-Performance Comparison 72

ABBREVIATIONS

PV Cells	Photovoltaic Cells
CSP	Concentrated solar power
RCT	River Current Turbine
VAWT	Vertical Axis Wind Turbine
HAWT	Horizontal Axis Wind Breaker
AOA	Angle of Attack
TSR	Tip Speed Ratio
RCECS	River Current Energy Conversion System
DMST	Double Multiple Stream tube Theory
CFD	Computational Fluid Dynamics
NACA	National Advisory Committee for Aeronautics
RANS	Reynolds Average Navier Stokes
FYP	Final Year Project

NOMENCLATURE

Symbol	Description	Unit
m	Mass	[kg]
α	Angle of Attack	[^{o}]
γ	Pitching Angle	[^{o}]
μ	Dynamic Viscosity	[kg/m^3]
ω	Angular Velocity	[rad/s]
ρ	Density	[kg/m^3]
θ	Azimuthal Angle	[^{o}]
A	Area	[m^2]
c_u	Dissipation Coefficient	[-]
b	Number of Blades	[-]
c	Chord	[m]
C_D	Drag Coefficient	[-]
C_L	Lift Coefficient	[-]
C_P	Power Coefficient	[-]
D	Diameter	[m]
F_D	Draf Force	[N]
F_L	Lift Force	[N]
F_N	Normal Force	[N]
F_T	Tangential Force	[N]
h	Height	[m]
l	Length	[m]

P	Power	[W]
p	Pressure	[N]
T	Torque	[Nm]
R	Radius	[m]
Re	Reynolds Number	[-]
Re_L	Local Reynolds Number	[-]
U	Free Stream Velocity	[m/s]
σ	Solidity	[-]
λ	TSR	[-]

1. INTRODUCTION

The study aims to standardize the design of vertical axis Gorlov turbines and implement a practical model to achieve a small-scale power output for low flow and low head conditions by exploiting the energy available in canals and open channel streams. Section 1 provides some background for this initiative, the problem statement and the objectives of the project. Section 2 focuses on the literature review. This includes a brief summary of previous works while expanding upon the feasibility of the current design selection and various design parameters. The literature review is followed by the design methodology in section 3. It focuses on the various design tools and modeling techniques used to aid the selection of the final design. The outcome of the calculations is presented in the next section. The results are validated by comparison with previous works and research. Further areas of improvements and recommendations are stated in the final chapter.

1.1. MOTIVATION

The world population is continuously rising and so is the energy demand. Half a billion increase is expected in population within the span of eight years. By 2050, population is expected to rise by 2 to 4 billion [1]. Moreover, higher consumption of energy due to urbanization has caused increase in energy demand. It is expected that by 2050, global urban population will increase by 2.5 billion [2].

Pakistan, like various other countries, is also suffering from acute energy crisis due to the two aforementioned reasons. In 2015, the nominal installed capacity of electricity generation in Pakistan was 24,961 MW whereas the generation capability at System Peak Demand was recorded to be approximately 19,000 MW [3]. Yet another important reason for the current energy crisis in Pakistan is the heavy dependence of power generation sector on fossil fuels. Pakistan imported 4.98 billion tons in year of June-March 2016, of which 34% alone was consumed by power generation sector. But since the oil prices fluctuate in the international market, Pakistan was often compelled not to purchase the desired amount of oil from the oil-producing countries, which has often led to further

widening of the demand-supply gap, up to the staggering figure of 7000 MW at one instant in 2015 [4].

Pakistan finds itself in the midst of a power crisis. These times call for an effort to exploit renewable energy resources. It has already found its way into mainstream energy generation methods as shown in the following figure. Renewable resources constituted a 19.3% share of the global energy generation and are compatible with the environment [5]. Therefore, they simultaneously contribute to increased energy efficiency, climate change mitigation and economic benefits.

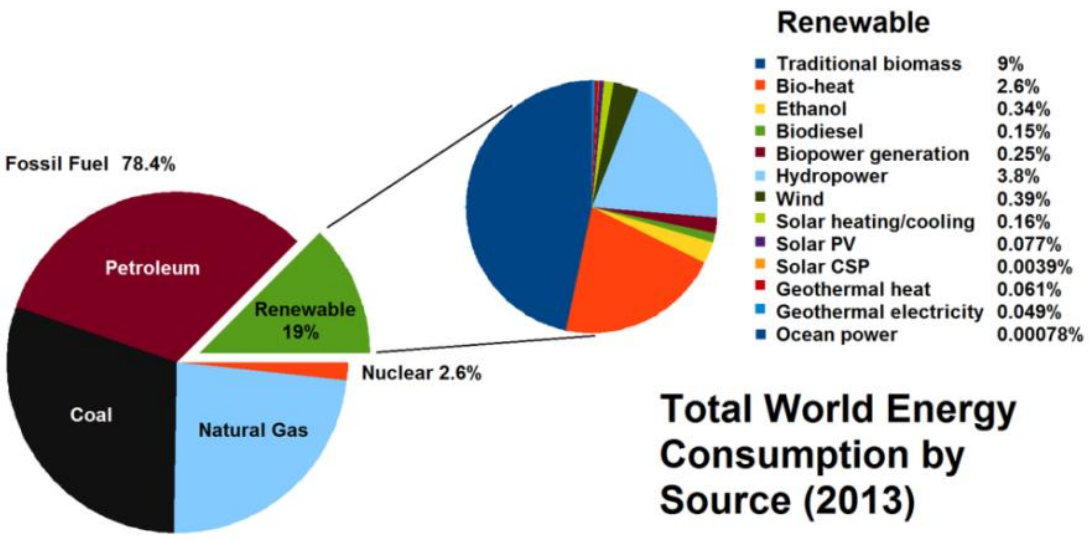

Figure 1-World energy consumption by resource [5]

Renewables can be classified as solar and non-solar [6]. The various types of resources that can be utilized are as follows

- **Solar Energy –** It can be used for direct heating of living spaces, power generation purposes, solar cooling and finds its application in a variety of commercial and industrial uses. It can be harnessed by using PV cells, CSP and artificial photosynthesis**.**
- **Wind Energy –** It is driven by the sun's heat as a result of the uneven heating and cooling of the atmosphere that creates a temperature difference driven flow. It can

be harnessed by using wind turbines with modern ones having an installed capacity of up to 9MW. Constant high speed winds present favourable condition for wind turbines since the power is a function of the cube of velocity. Offshore sites provide a greater potential for exploitation in the future and may increase the energy production by almost five times the current installed capacity.

- **Hydro Energy –** It involves the utilization of energy stored in water. It can be harnessed using turbines, for instance, impulse turbines utilize the potential energy of water and reaction turbines utilize the kinetic energy of water. Wave power (which involves harnessing the energy of the surface waves) and tidal power (which involves harnessing energy from the tides) provides two potential avenues for future exploitation.

1.1.1. Hydro Energy

Renewable resources constituted a 19.3% share of the global energy generation with hydro-energy making up approximately 4% of this share. Among the various options, hydro-energy is right up there in terms of potential for energy extraction. It is estimated that Pakistan's hydro-energy reserves have a potential of about 60,000 MW but only 11% of the total capacity serves as a source of energy [7]. According to a conservative estimate, the total energy potential of Kachhi Canal amounts to 85.3 kW which qualifies it as a micro hydro energy prospect [8]. Since dams are prohibitively expensive, we need to tap into Pakistan's intricate canal network to harvest energy in a sustainable and cost-effective way.

Pakistan Council of Renewable Energy Technologies and Alternative Energy Development Board are the prime institutions responsible for fostering the growth of renewable energy sector. The Government of Pakistan is using various fiscal and financial incentives to attract the investors to power generation via renewables, such as provision of soft loans from State Bank of Pakistan and reduced licensing fees for renewable projects [9].

1.2. PROBLEM STATEMENT

Turbines can be categorized on the basis of installed generation capacity. Micro hydro turbines are small scale turbines with a low generation capacity of up to approximately 5-100kW. Below this capacity are pico turbines. These small hydro installations can be used in remote areas for powering residents of the locality. These turbines provide a viable and appealing alternative to solar power generation methods when conditions are not conducive. The installations are used in streams and small rivers.

The canals of Pakistan provide a promising outlet for power generation; however, conventional solutions cannot be implemented. The challenge therefore is to develop a turbine that operates under low flow and low head conditions and is capable of exploiting these conditions with a high degree self-starting capability. Therefore the need to artificially generate a head is eliminated since the turbines under study utilize the kinetic energy of the flowing medium. Moreover, since the density of water is almost 800 times to that of air, power generation potential is promising even at low speeds.

1.3. OBJECTIVES

The project aims to incorporate analysis to select a blade design for turbines with ab balance between optimum power generation and improved self-starting capabilities. Simulations will be carried out to deduce the power output, and further will be verified by testing of the fabricated small-scale prototype in a canal.

The turbine will have the added benefit of easy installation without the need of water proof generator or complex manufacturing processes. The manufactured turbine will operate on the designed TSR which is set according to flow conditions to get peak performance. The effect of the following parameters on the performance is studied:

- Solidity
- Number of Blades
- Aspect Ratio

2. LITERATURE REVIEW

The background research into turbines proved essential in converging upon a single design configuration for optimal performance under proposed conditions. The principles of harnessing energy from the turbine and performance parameters were researched comprehensively.

A turbine is a machine that produces power in a continuous manner by the revolution of a wheel or rotor, usually having vanes, using a fast-moving flow of gas, steam, water, air or any other fluid. On the basis of flowing fluid type commonly the turbines are either wind turbine or water turbines (also known as hydro turbines).

2.1. HYDROKINETIC TURBINES

A hydro turbine is used to convert the hydro energy (kinetic energy of water) into electrical energy with the help of a generator. The turbine extracts the energy from water and transforms it in mechanical energy. This mechanical energy is then utilized to derive a generator to produce electricity.

Hydrokinetic turbines is defined as Low pressure run-of-the-river ultra-low-head turbine that will operate on the equivalent of less than 0.2 m of head [11]. These turbines provide an easy solution to extract energy from free stream water channels and are becoming main stream due to economic feasibility and commercialization capability.

The two main areas where hydrokinetic turbines can be used for power generation: Tidal current applications and River stream applications. Hydrokinetic turbines which are deployed in rivers are known as river current turbines (RCT) or river current energy conversion system (RCECS).

2.1.1. Advantages

There are various advantages offered by the hydrokinetic turbines. These include their higher efficiency, easy installation and lower initial investment.

Efficiency

They can generate power from limited flow rates thereby indicating a high efficiency in operation.

Continuity

These turbines can provide a consistent source of power year-round when compared with other renewable energy resources.

Assembly

They do not require complex arrangements. Moreover, since they allow the water through, they have a minimal impact on the environment.

Cost

Initial costs are lower due to simple construction and a fairly simple assembly makes maintenance simple and inexpensive. They also provides a promising avenue for implementation in undeveloped countries and remote areas of the world.

2.1.2. Limitations

Some of the disadvantages of hydrokinetic turbines in general are mentioned below:

Site Condition

Terrain plays and important role in installation. Some important factors impacting the installation include distance from the power source, flow rate of the stream and size of the water body

Increase in demand

The physical size and the water velocities in the streams limit the power output of the micro hydrokinetic turbines.

Inconsistency in flow rate

Throughout the year, the water flow rate will never remain consistent and will result in the reduction of the total power output of the micro hydrokinetic turbines.

2.2. NEED FOR HYDROKINETIC TURBINES

Hydropower is among the cheapest renewable energy sources. Conventionally dams have been used as the single most dominant outlet in harnessing energy. However, as the prevailing situation suggests, the dams in Pakistan are not sufficient to fulfill our energy needs and overcome the supply-demand gap. Economic feasibility and timescale restrictions do not project dams as a viable solution to meet our energy needs.

Pakistan has a large number for small water channels, streams and rivers on the northern side of the country. Moreover, an intricate water system of 12 link canals and 45 normal canals, provide enormous potential that can be exploited for energy generation. These low head reservoirs provide a capable resource. Low head hydropower applications aims at harnessing this energy potential. This avenue provides a low cost alternative to dams that can be easily implemented in remote areas and off-grid locations.

2.3. TYPES OF TURBINES

2.3.1. Mechanism Used to Harness Flow Energy

The categorization is based on principle of operation, specifically the mechanism used to harness energy potential of the water body.

Savonius Turbine

These turbines are also referred to as ***impulse*** turbines or ***drag-type*** turbines. These turbines use the velocity of the water to move the runner and discharges to atmospheric pressure. The water pushes on the curved blades which changes the direction of flow. This brings about a change in momentum of the blades resulting in a force. The name of the turbine is derived from this principle.

Low Tip Speed Ratio (TSR) values for drag based devices indicate a high degree of inefficiency for this configuration although the self-starting characteristics provide a more favourable outlook for operation under low head. This is the reason why the drag

type devices are generally used for low power applications. Savonius hydrokinetic turbines can be deployed in regions even with very low flow rates with ranging flow velocities from $0.5ms^{-1}$.

These turbines are suitable for high head, low flow applications since the high potential energy of the flow can be converted to kinetic energy. Example includes the Pelton wheel. Impulse turbines tolerate sand, are easy to fabricate, efficient at wide a range of head and flow. Nozzle converts pressurized water into a high-speed jet of water.

Darrieus Turbine

These turbines are also referred to as ***reaction*** turbines or ***lift-type*** turbines. A reaction turbine generates power from the combined action of pressure and moving water. The runner is placed directly in the water stream flowing over the blades rather than striking each blade individually. A reaction turbine doesn't change the direction of the fluid flow as drastically as an impulse turbine: it simply spins as the fluid pushes through and past its blades.

Lift is generated due to the distribution of pressure on the airfoil surface. Different curvatures of top and bottom of airfoil lead to a difference in the lengths of path by air over foil. These turbines produce motive force required for rotation by making use of the lift generated due to the flow of water around the blades of the turbine at an angle relative to the blade chord known as angle of attack. The surface drag forces are easily overcome during the operation of the turbine.

Reaction turbines must be encased to contain the water pressure or fully submerged in the flow. Their principle of operation is based on Newton's third law. They are used in low (<30m) and medium (30-300m) head application with high flows.

These devices operate at TSR of greater than unity. The RPM of the turbine is consequently greater and coupling with the generator does not involve high gear ratios. This subsequently decreases mechanical losses.

2.3.2. Orientation of Turbine Relative to Flow

The categorization is based on the direction of the axis of rotation relative to the flow direction. The details are as follows.

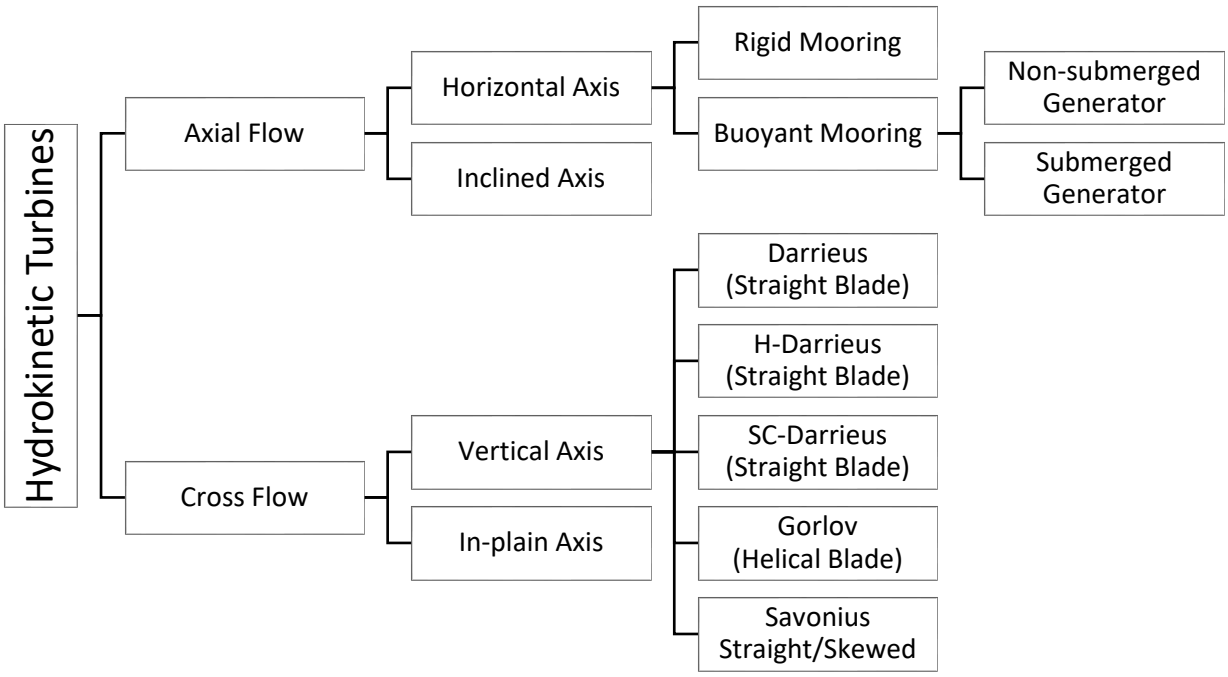

Figure 2-Classification of hydrokinetic turbines

Axial flow turbines

Rotational axis of the rotor is parallel to the incoming flow stream employing lift or drag type blades. They may consist of two, three or multiple blades in differing orientations. They are mostly configured in horizontal configurations.

Cross flow turbines

Rotational axis of the rotor is orthogonal to the stream flow. It can be further classified as

- In-plane axis turbine – Axis is parallel to the surface of the water body
- Vertical axis turbine – Axis is perpendicular to the surface of the water body. The assembly can be fully or partially submerged in water.

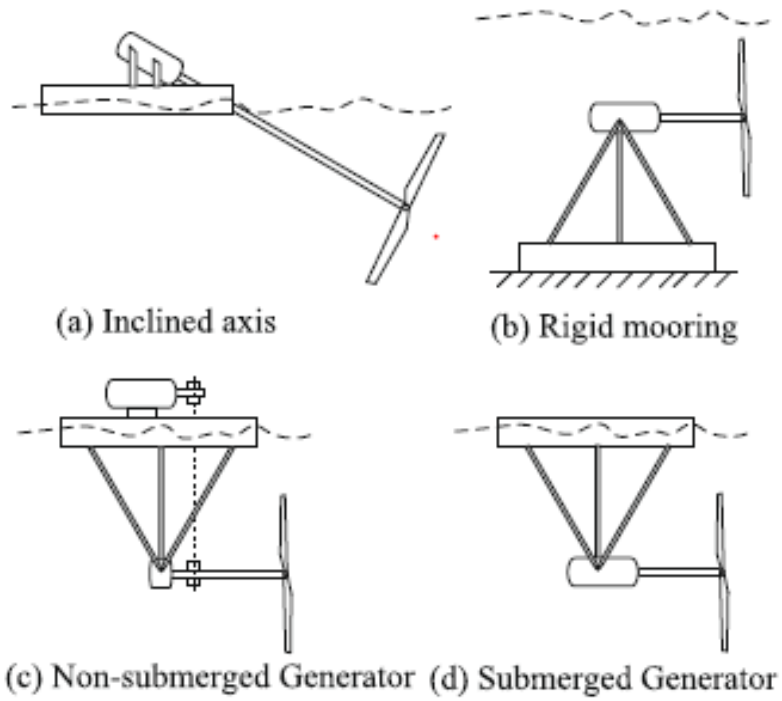

Figure 3-Axial flow turbines [12]

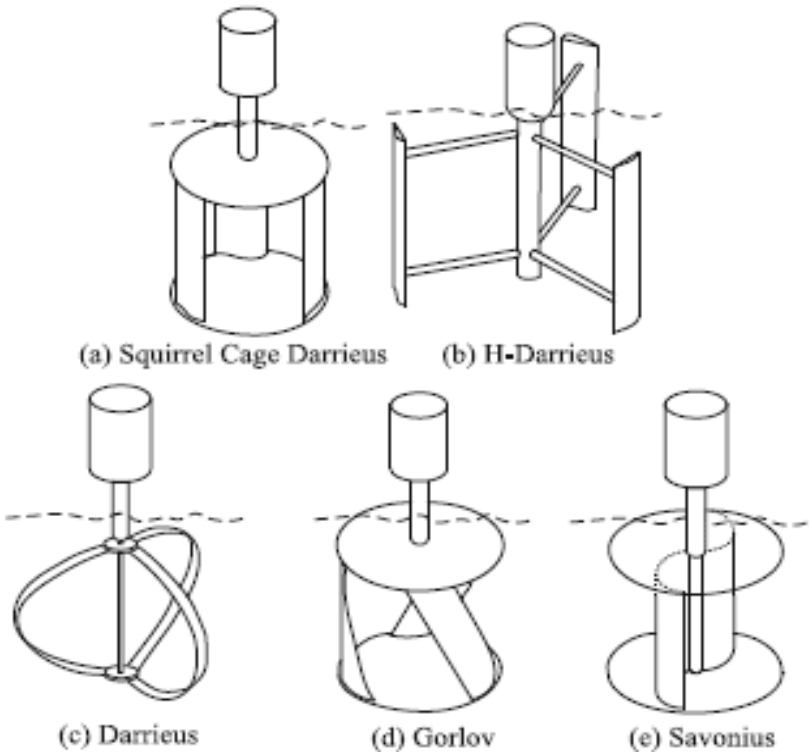

Figure 4-Cross flow turbines [12]

Amongst the aforementioned configurations, the most commonly used orientations are ***Horizontal Axis*** (a type of axial flow turbines) and ***Vertical Axis*** (a type of cross flow turbines) configurations. The technical merits and disadvantages of various turbine types were compared comprehensively.

Table 1-Design comparison [8]

	Horizontal Axis Configuration	**Vertical Axis Configuration**
Design Simplicity	These have blades that involve delicate machining and high cost of manufacturing	Have relatively simple structure of blade that are economically more feasible
Generator Coupling	Involves complex challenges like gear couplings, inclined shaft for transmission and underwater generator.	Simpler as allows easier extension of the shaft, enabling the generator to be placed above the submerged assembly.
Skewness of Flow	These cannot cope with the water velocity variations in vertical direction, as the upper part of the turbine faces higher velocity than the lower section.	These are better equipped to operate in shallow conditions since each blade experiences same force at an angle of attack

2.4. DESIGN SELECTION

2.4.1. Mechanism of Operation

Having higher efficiency, the Darrieus turbines were more preferred over the Savounis type. Darrieus configuration, however, has poor self-starting characteristics and torque fluctuations do not bode well for structural integrity of the blades.

These issues are catered for by adopting a ***Helical Grovel configuration***, a unique type of Lift-Based turbine. This turbines couples the advantages of a typical Darrieus turbine with additional benefits including has low ripple factor, as well as better self-starting characteristics due to lower head requirements [13].

2.4.2 Orientation of Turbine Relative to Flow

After a thorough analysis, the horizontal axis design was not considered due to following reasons:

- Higher cost of setup due to insulation requirements of the generator and transmission losses. This may also lead to system inefficiencies.
- Their requirement to be properly aligned to direction of flow to achieve peak performance.
- Difficulty in deployment in small rivers.
- It cannot be stacked. Only allows single unit installation ability
- Lack of ability to deflect debris which affects operation

Hence, the final decision was to work on selecting the optimum parameters of a ***Vertical Axis Gorlov (Helical type) Lift-Based Turbine***.

The following sections now will discuss the design methodology employed to develop a turbine with a balance between efficiency and self-starting capability.

3. ANALYTICAL MODELING

3.1. BASICS OF TURBINE PERFORMANCE ANALYSIS

The Darrieus turbines operate on the forces generated by turbine due to the shape of the airfoil. The two types of forces involved in this mechanism are Lift and Drag forces.

Frictional drag occurs because of the presence of shear stresses on surface and enhances with increase in viscosity. Raising the Reynolds number though, which is inversely proportional to viscosity, will lower the frictional drag.

The formation of these forces is explored further with the help of the following diagram

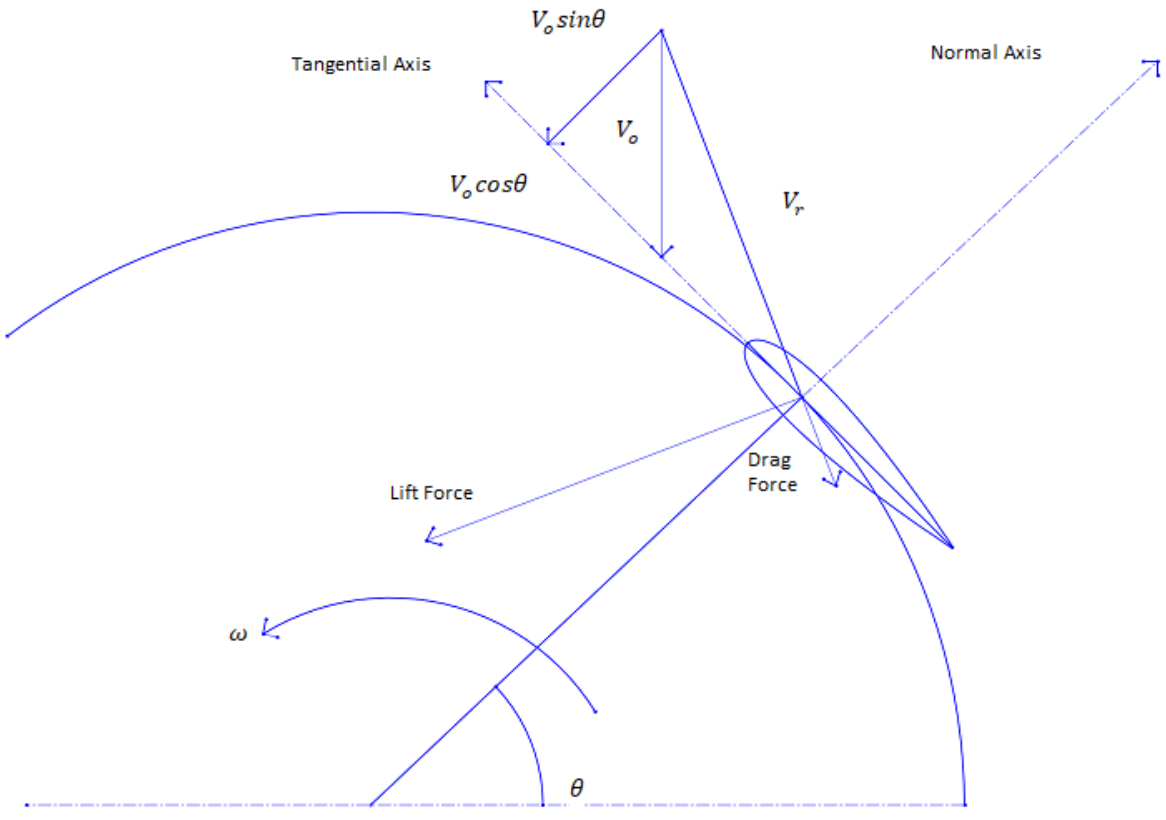

Figure 5-Forces on an airfoil section [14]

The relative velocity is found by the vector sum of the tangential and normal velocity components as shown below:

$$V_R = \sqrt{(V_a sin\theta)^2 + (V_a cos\theta + \omega R)^2} \quad \textbf{(1)}$$

Where,

V_R = relative velocity at turbine blade

V_a = absolute velocity at turbine blade

ω = rotational velocity

R = radius of turbine

θ = azimuthal angle

Simplifying further leads to

$$\frac{V_R}{V_\infty} = \sqrt{(\frac{V_R}{V_\infty} sin\theta)^2 + (\frac{V_R}{V_\infty} cos\theta + \frac{\omega R}{V_\infty})^2} \quad \textbf{(2)}$$

$$\frac{V_R}{V_\infty} = \sqrt{((1-a)sin\theta)^2 + ((1-a)cos\theta + \lambda)^2} \quad \textbf{(3)}$$

This has helped to express the ratio of relative and free stream velocity as induction factor '*a'* and Tip Speed Ratio 'λ'.

The angle of attack α can be expressed as

$$\tan\alpha = \frac{V_a sin\theta}{V_a cos\theta + \omega R} \quad \textbf{(4)}$$

$$\tan\alpha = \frac{\frac{V_a}{V_\infty} sin\theta}{\frac{V_a}{V_\infty} cos\theta + \frac{\omega R}{V_\infty}} \quad \textbf{(5)}$$

$$\alpha = \tan^{-1}\left(\frac{(1-a)sin\theta}{(1-a)cos\theta + \lambda}\right) \quad \textbf{(6)}$$

The normal force C_n and tangential force C_t can be found using the following equations.

$$C_n = C_L \cos\alpha + C_D \sin\alpha \quad \textbf{(7)}$$

$$C_t = C_L \sin\alpha - C_D \cos\alpha \quad \textbf{(8)}$$

Finally, the two most important

$$T = \frac{1}{2}\rho {V_R}^2 (hc)(C_t \cos\theta - C_n \sin\theta) \quad \textbf{(9)}$$

where h is the height of blade and c is the chord length.

The power is given as

$$P = \frac{1}{2} C_p \rho \pi R^2 U^3 \quad \textbf{(10)}$$

3.2. DOUBLE MULTIPLE STREAM MODEL

One of the analytical modeling approaches employs the use of momentum models for evaluating the turbine performance. For a hydrokinetic turbine, the change in momentum after the fluid moves past the turbine leads to power generation. This forms the basis of

these theories. The theories, in essence, work on the three mail governing equations (mass, momentum and energy) written below:

$$\frac{d}{dt}\int \rho \, \mathrm{dV} + \oint \rho U \cdot n \, \mathrm{dS} = 0 \tag{11}$$

$$\frac{d}{dt}\int \rho \, \boldsymbol{U} \, \mathrm{dV} + \oint \rho \, \boldsymbol{U} \, (u \cdot n) \, \mathrm{dS} = \sum F_{ext} \tag{12}$$

$$\frac{d}{dt}\int \rho \, \boldsymbol{U}^2 \, \mathrm{dV} + \oint \frac{1}{2}\rho \, \boldsymbol{U}^2 \, (U \cdot n) \, \mathrm{dS} = -P \tag{13}$$

The simplest of these is the single stream tube model. In this model, the turbine is assumed to be a thin actuator disc, and there is only one tube of free stream fluid. In the multiple stream models, it is assumed that the induction factor may vary in the direction perpendicular to the wind, but is constant in the direction of the wind.

Double multiple stream tube theory is a derivative of the multiple stream tube theory. It builds upon the principle that downstream flow is affected by the obstruction experienced by the upstream flow. Therefore, two actuator discs are used to model each half stream; the upstream blade pass and the downstream blade pass.

3.3. Q-BLADE

Q-Blade is a turbine calculation tool developed by Technical University of Berlin to evaluate performance of various Horizontal-Axis and Vertical-Axis Turbines. This modeling software employs Double Multiple Stream Theory to evaluate the performance of turbine by predicting the Coefficient of Performance and Coefficient of Torque. It also integrates XFOIL facility developed at MIT that allows user to design custom airfoils. Q-Blade has been employed by researchers in various renowned peer-reviewed journals, including Energie (Impact Factor: 2.201).

The following diagram shows one of the turbines modeled in Q-Blade. Each turbine was divided into 40 elements for optimum results.

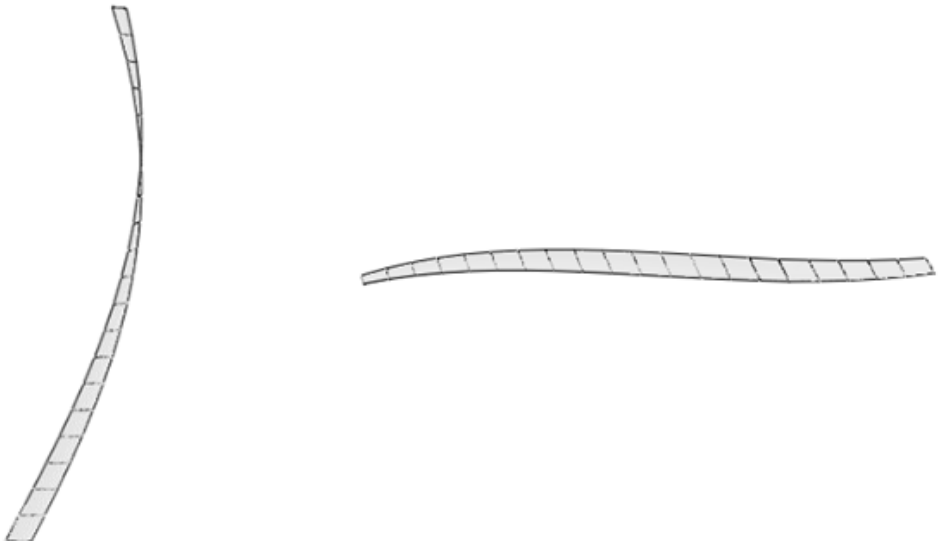

Figure 6-Turbine blade based on NACA Airfoil

3.4. DESIGN PARAMETERS

The following section describes the parameters that affect the turbine performance. Iterations were carried out by altering the values over a certain range to find the best possible design for the desired input conditions. In each case, Q-Blade was employed to conduct simulations and predict the turbine performance.

3.4.1. Blade Profile

Airfoil

Airfoil is such a cross sectional streamlined shape that when it moves through a medium, the medium is split and passes above and below the wing. The upper contour is shaped so that the speed increases and pressure decrease above the wing. The fluid flowing below the wing moves relatively unobstructed, so its speed and air pressure do not vary. This pressure differential across the upper and lower surfaces causes the air below the wing to

push upward toward the air above the wing. The wing is in the middle, and the whole wing is lifted.

NACA Airfoil

The NACA airfoils are airfoil shapes for aircraft wings developed by the National Advisory Committee for Aeronautics (NACA). The shape of the NACA airfoils is described using a series of digits following the word "NACA". The parameters in the numerical code can be entered into equations to precisely generate the cross-section of the airfoil and calculate its properties.

The NACA four-digit wing sections define the profile [15]. For example, the NACA 2412 airfoil has a maximum camber of 2% located 40% (0.4 chords) from the leading edge with a maximum thickness of 12% of the chord. The NACA 0015 airfoil is symmetrical, the 00 indicating that it has no camber. The 15 indicates that the airfoil has a 15% thickness to chord length ratio: it is 15% as thick as it is long.

Comparative Study

Three airfoils were considered for analysis, which were NACA 0012, 0015 and 0018 respectively. All of them have a symmetrical profile. The relative profile arrangement is illustrated as follows

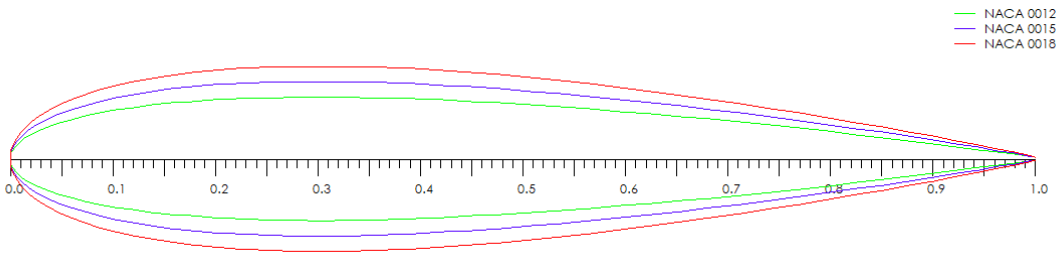

Figure 7-Airfoil profile comparison

Design Selection

For our analysis, NACA 0018 airfoil was considered, due to the availability of complete data and optimum lift generation for driving turbine.

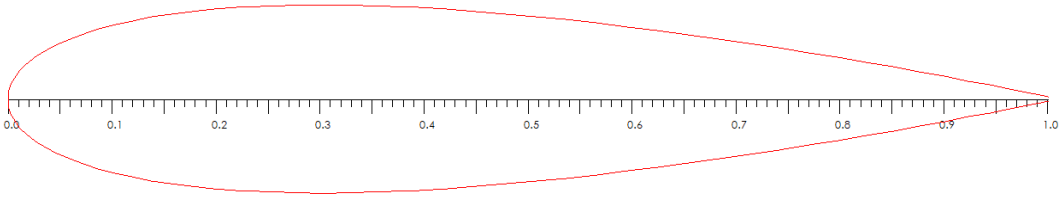

Figure 8-NACA 0018 Airfoil in Q-Blade

Non-symmetric airfoils were not considered due to unpredictability of flow and the inability of the cambered profile to deal with such conditions. They work better at low angles of attack to generate lift however affect the performance of the turbine over the complete cycle. The rest of the profiles were not optimized with respect to self-starting capability of the turbine. The comparative analysis of blade profile performance is given below. 0018 provides the most stable performance for the chosen configuration.

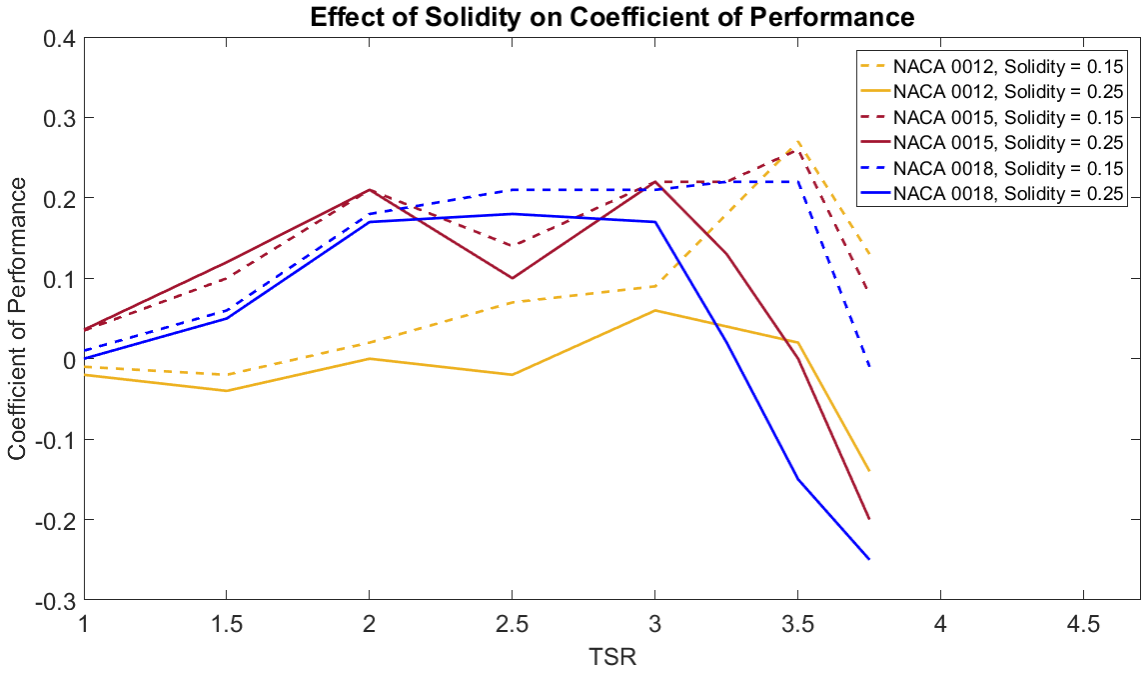

Figure 9-Comparative Analysis of Profile Performance

3.4.2. Number of Blades

As mentioned previously, a baseline value of solidity was selected to serve as the foundation of the design. However, the desired solidity can be achieved by varying the chord length and number of blades in an inverse manner.

A single blade would be the ideal choice due to least resistance to flow. However, a complete blade wrap is next to impossible and would cause imbalance in operation. The blade wrap problem also comes up in two bladed turbines.

A higher number of blades provides a greater resistance to flow and decreases the efficiency of operation at higher speed because of flow separation hence the peak power is achieved at lower speed. This was also observed as a result of simulations carried out on Q-Blade. However, as the number of blades is increased the design approaches a straight blade configuration thereby increasing efficiency. Therefore, a four bladed design provided an optimum compromise.

The model generated in Q-Blade is shown in Figure 10. It can be seen that the blade elements cover the complete circumference of the circle when viewed from the top. This is discussed in the following sections.

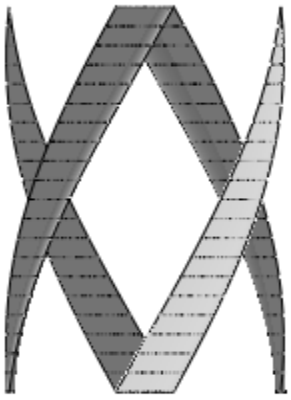

Figure 10-Turbine model generated in Q-Blade

The following graph predicts the improved performance of 4-blade turbine as compared to 3-blade turbine at lower speed, an important consideration in our design selection.

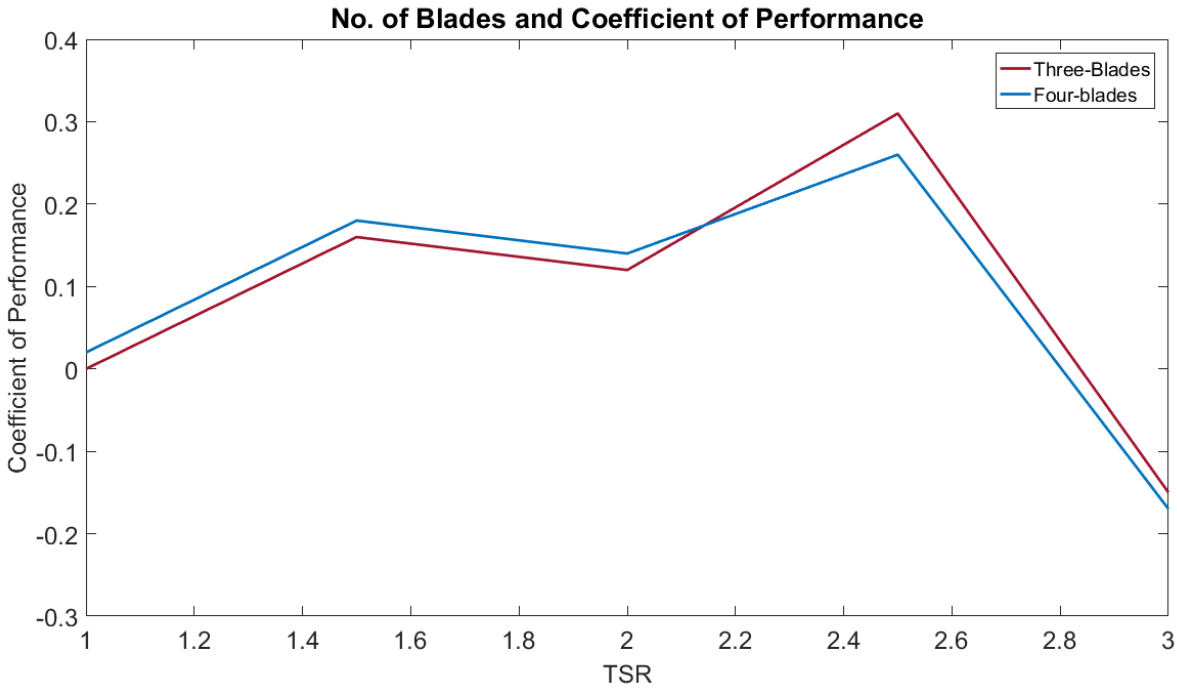

Figure 11-Effect of number of blades on turbine performance

3.4.3. Blade Wrap

Blade wrap is the amount of the circumference of the turbine that is covered by the blades. In straight blade Darrieus turbines, the blades are at a specific angle of attack at any instant of time. During operation, as the turbine rotates, the angle of attack of the blade changes for every cross section of the blade. This results in a sudden torque variation which is called the torque ripple. This phenomenon affects the output power to the source.

In a Gorlov helical turbine, the blades are twisted so as to wrap around the turbine (hence the name 'blade wrap'). Due to this, at least one blade cross section is at an optimum angle of attack during the complete 360^{o} motion of the turbine. This reduces the torque ripple and enhances self-starting characteristics by provide a sufficient frontal area for water impact and start up motion.

The blade wrap value was chosen to be 100%. This ensures smooth torque transmission and power output. This also improves the structural integrity of the turbine since the blades are now subjected to a lower or negligible degree of fatigue loading.

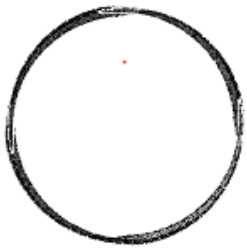

Figure 12-Top view of turbine model

3.4.4. Solidity

Solidity is defined as the ratio of total blade chord length to chord circumference. This is given by the formula

$$\sigma = \frac{b * c}{2\pi R} \quad \textbf{(14)}$$

Where

σ Turbine solidity

b Chord length (m)

c Number of blades

R Radius of the sweeping area of the turbine (m)

Different iterations were conducted for values from 0.15 to 0.35. An increase in solidity meant better self-starting characteristics, but at the expense of lower coefficient of performance beyond a certain point.

High C_p values were obtained for lower solidities. This would however come at a cost of the self-starting capability of the turbine. Therefore, an intermediate value at 0.28 for the solidity was selected as the base value to serve as the foundation of the design.

The results show that as the aspect ratio is increased, the value of coefficient of performance for a specific solidity also increases. The trend for various values is illustrated in the graph below.

3.4.5. Aspect Ratio

Aspect Ratio is the ratio between the height and the diameter of a turbine, as suggested by the formula

$$\text{Aspect Ratio} = \frac{h}{D} \tag{15}$$

Multiple cases explored for values ranging from 1 to 2.25. Higher aspect ratios enhanced the **power coefficient** of Turbine, but at the expense of the **starting torque coefficient** produced if the height is kept constant.

Moreover, a lower aspect ratio ensured better structural integrity in preventing failure of blades due to stresses induced by hydrodynamic forces. This also represents a trade-off between durability and performance.

The iterations also depict that for same values of aspect ratio and solidity, the Coefficient of Performance vs. TSR graph stays unaltered for any dimensional values. Thus, the turbine design was non-dimensionalized for two parameters. This is illustrated as follows

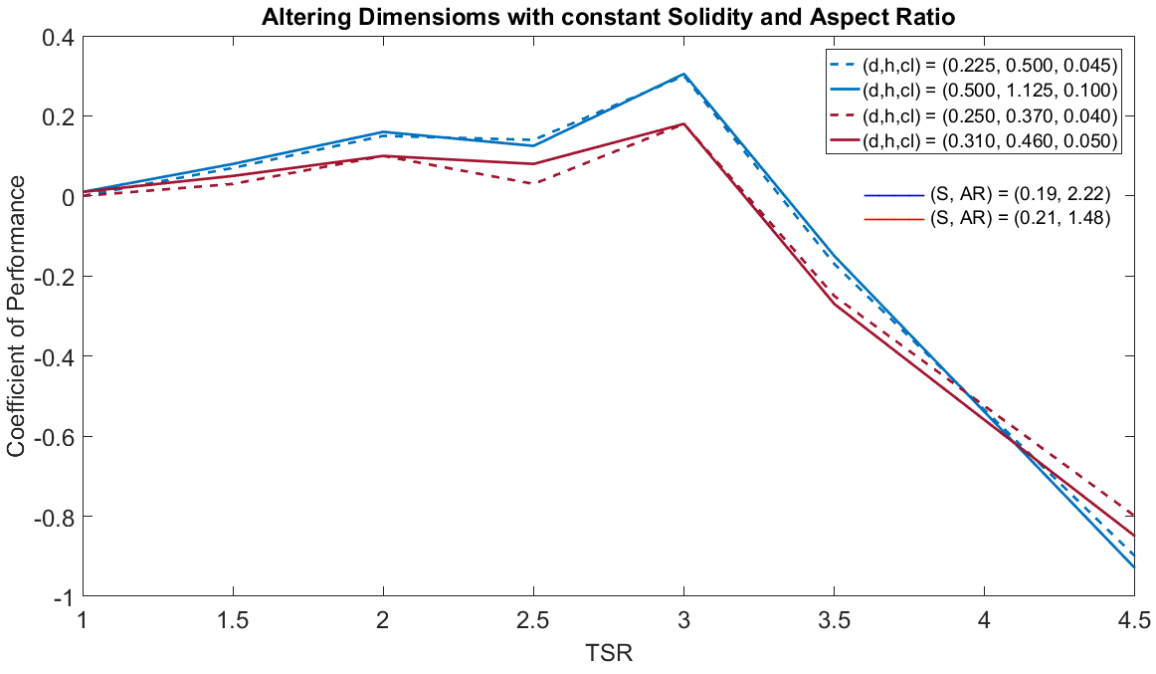

Figure 13-Non-Dimensionality Analysis

3.5. CONCLUSION

After conducting various simulations in Q-Blade, it was agreed to design a 3-blade turbine with NACA 0018 Airfoil with chord length of 5.5 cm. The dimensions of turbine include height 0.38m, diameter 0.25m, Turbine Aspect Ratio of 1.52 and solidity of 0.29. This will produce a maximum torque of 4.3 Nm with power output of 63 W.

Table 2-Final turbine parameters

Turbine Design	
Height	0.38 m
Diameter	0.25 m
Aspect Ratio	1.52
Number of Blades	4
Solidity	0.29

The NACA 0018 foil was used. The final parameters are presented in the table below

Table 3-Final blade parameters

Blade Parameters	
Type	Symmetrical
Height	0.38 m
Chord Length	0.055 m
Blade Wrap	100%

Based on the above-mentioned dimensions, a 3D CAD designed model was created in SOLIDWORKS and a 3D CFD analysis was carried out to verify the results from Q-Blade Analytical Modeling.

4. CFD ANALYSIS

4.1. IMPORTANCE OF CFD ANALYSIS

Computational Fluid Dynamics finds its basis in handling complex flows by adopting a numerical approach to model real life scenarios. The numerical solution, even though it remains approximate, has achieved increasing degree of accuracy in recent decades with the advent of high speed computing technology.

The purpose of conducting CFD Analysis was ***to validate the simulations conducted by Q-Blade Software***. Q-Blade was the most preferred option since it offered two essential advantages to us in our design phase: reduction in simulation time and low cost computational resources. Hence, before conducting a detailed simulation analysis using Q-Blade, a CFD analysis was initially conducted to compare the results of the two software using same parameters. Similar designs were used and results were compared to determine the feasibility of Q-Blade software.

4.2. CREATION OF GEOMETRY

The CAD model generated for test analysis is as follows

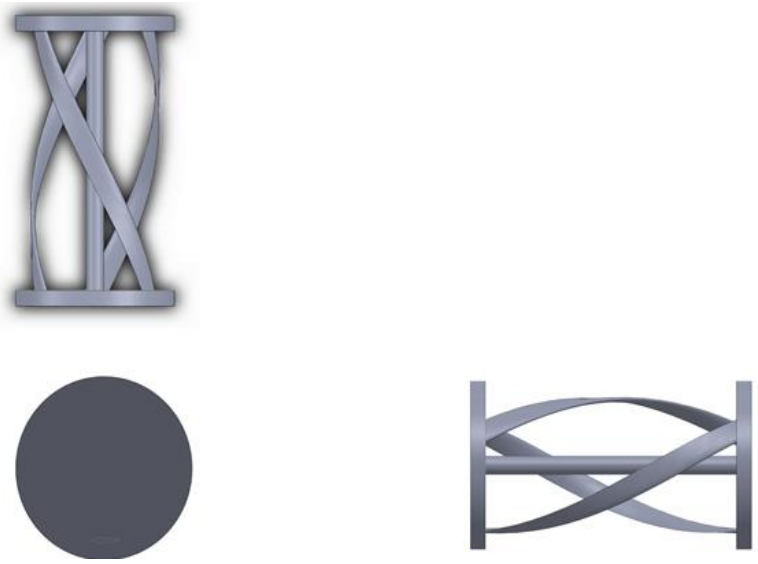

Figure 14-CAD Model

4.3. MESH DEFINITION

Following table represents the number of nodes produced for each element size. The size of turbine elements was varied from 9 mm to 5 mm in each simulation, producing a trade-off between computational time and resources, and quality of mesh.

Table 4-Number of Elements, Nodes and Y-Function for corresponding Body Size

Mesh No.	Mesh Element Size (m)	Elements	Nodes	Orthogonal Quality	Skewness	Aspect Ratio	Y-Function Value
1	0.009	2,938,334	538,648	0.76379	0.235	1.8641	350
2	0.007	3,333,498	611,206	0.76771	0.231	1.8536	260
3	0.006	3,814,931	698,217	0.76981	0.229	1.8507	225
4	0.005	4,777,821	871,405	0.7732	0.225	1.8438	200

Following diagrams show a comparison of different meshes generated using different blade elements (mesh element) sizes. It can be observed that as the Mesh Element Size is decreased, the number of elements on the turbine increased.

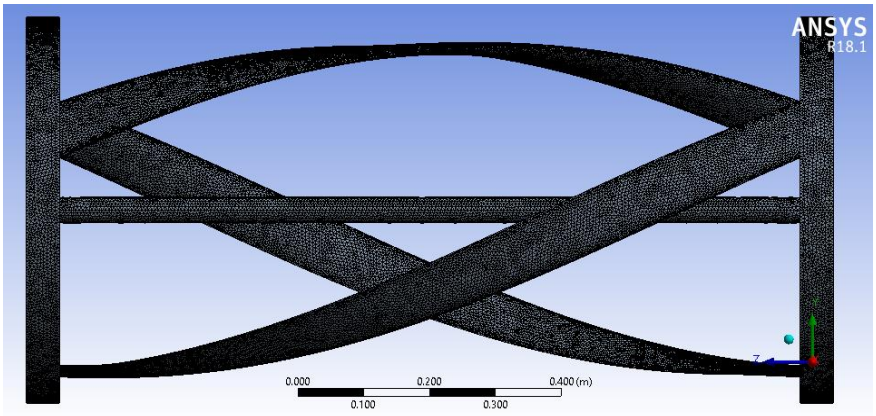

Figure 15-Mesh for Body Size: 5mm

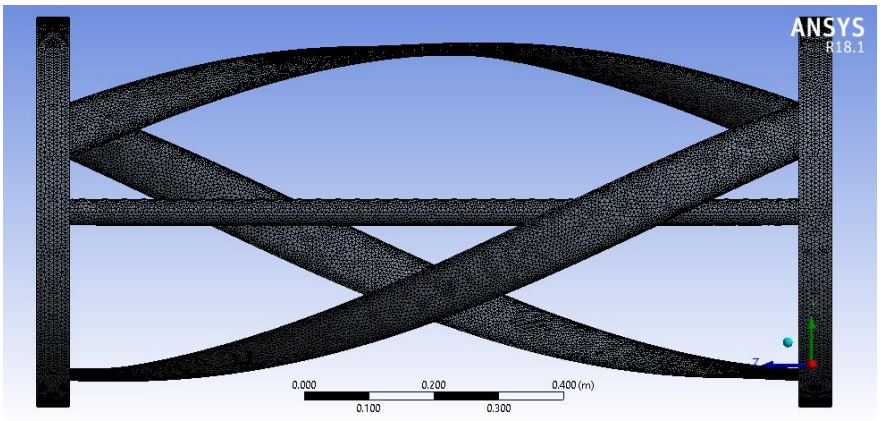

Figure 16-Mesh for Body Size: 6mm

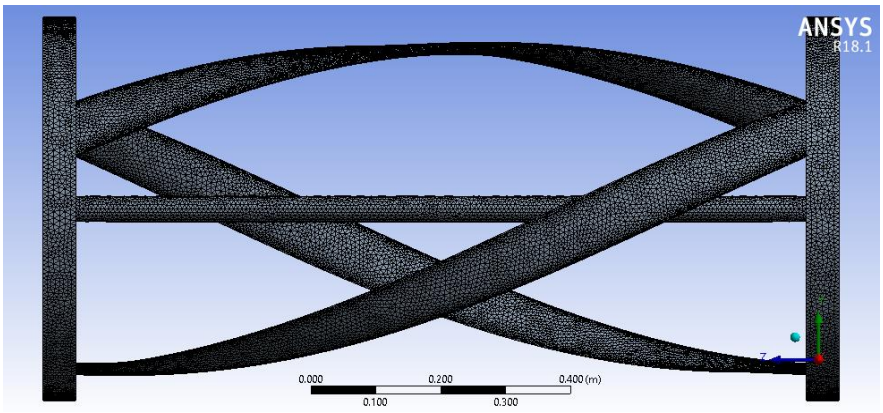

Figure 17-Mesh for Body Size: 7mm

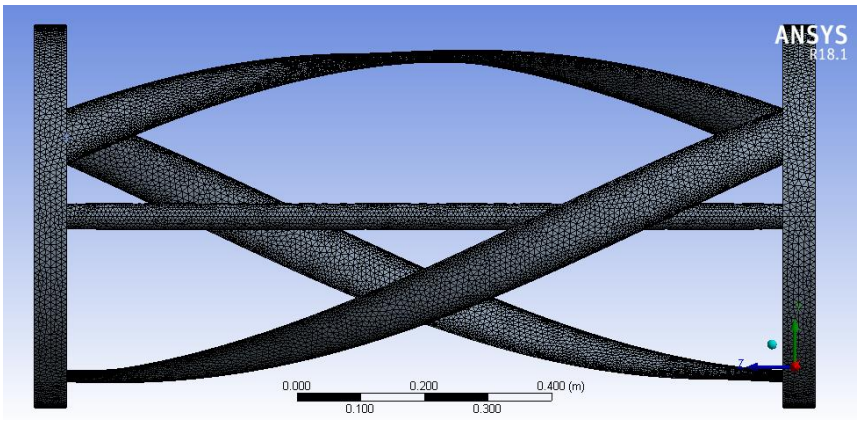

Figure 18-Mesh for Body Size: 9mm

The more refined mesh, the more accurate results are expected to be attained but at the cost of computational resources. Considering the limitations of the available

infrastructure, it was agreed to use the minimum element size to be 5mm.

4.4. SOLVER SELECTION

CFD simulations were carried out using Fluent – the ANSYS Module. An unstructured meshing approach has been adopted.

The following parameters were determined to ensure maximum degree of accuracy in the analysis

- Time Step

$$t = \frac{b}{10 * \omega} \quad \textbf{(16)}$$

- Turbulence kinetic energy

$$k = 1.5\left(U_{avg} I\right)^2 \quad \textbf{(17)}$$

- Turbulence dissipation rate

$$\epsilon = c_u^{0.75} \frac{k^{1.5}}{l} \quad \textbf{(18)}$$

4.4.1. Solver Analysis

Several different models were available for CFD Analysis, such as Reynolds Stress Model (RSM), Spalart-Allmaras Model, k-ω model or k-ε model. Here, k represents turbulent kinetic energy, ε represents the rate of dissipation of kinetic energy and ω is the specific rate of dissipation of kinetic energy.

Spalart-Allmaras Model uses a single turbulence equation for solving the CFD model. This allows it to yield convergence even with poor mesh quality. However, the use of

single equation prohibits the proper development of turbulent time scale and turbulent lengths if compared to the other models.

Next, the RSM approach was evaluated for our design. RSM Model attempts to directly solve the Reynolds-averaged Navier-Stokes (RANS) and also captures swirling flows. However, for our analysis, this was not used because it requires very high computational power, and it desires very high-quality mesh which further needs high memory (RAM).

Another option was to go with the k-ω model. This approach generally caters for better capture of the near-wall interactions. Again, this model was also not preferred due to the following reasons

- The convergence of this model is much difficult than the k-ε model
- The model is extremely sensitivity to the initial conditions

Hence, we finally opted for the k-ε model. This allows us to solve for accurate results with good convergence and moderate use of computational resources and memory [16]. In addition to this this model also does not present any problems with the free stream flows. Moreover, this model is also only scarcely sensitive to the inlet conditions – a prevailing issue with the k-ω model. Standard initialization was used to predict better initial values.

4.5. THE WALL FUNCTION APPROACH

During a CFD analysis the placement of our first node is very important. If we place our first node at a larger distance from the wall inflation than there is a chance that we'll not be able to capture the entire result of the phenomenon happening in the boundary region as a result error will be induced in our calculations. The arbitrary non-dimensional distance from the wall to our first mesh node is called +y. This distance is extremely important to our CFD analysis and will be chosen according to the type of flow we expect to encounter in our analysis. For instance, if we have a flow with a very high Reynolds Number then the boundary layer will extend up to thousands of +y units, while in case of

flow with low Reynolds Number the boundary layer will only extend up to a few hundred +y units [17].

If you have an attached flow in your CFD analysis, then the wall function approach is adopted for the analysis. This means that a large +y value can still be used for smaller overall mesh count. For our turbulence model we can have two approaches one is the wall function approach and the other is +y approach. The use of each approach depends upon the type of flow we are encountering.

The good estimate for the +y value can be calculated as follows.

$$\Delta y = L * y^{+} * \sqrt{74} Re_{l}^{\frac{-13}{14}} \quad \textbf{(19)}$$

Where,

Δy	=	Distance of the first node from the wall.
L	=	Flow characteristics Length Scale.
y+	=	Desired Value.
Re_l	=	Reynolds Number.

4.6. FLUENT MODEL

The following diagram shows the development of the CFD Setup for the model with element size of 5 mm. The domain size was carefully selected in order to avoid non-physical reflection of results such as:

- Fluid re-entering into the domain
- Region of large gradients and pressure and velocity changes

In order to accommodate these factors and to ensure the validity of boundary conditions an appropriate domain size was chosen [18]. The dimensions of the domain are listed as:

- Length 32xR
- Height 12xR

- Width 12xR

Where ‘R’ is the radius of the turbine

For the next phase, the **data and figures** for the **model with element size of 5 mm** are represented since the results yielded by this model were the most accurate. The rest of the images are not added to keep the report concise and avoid mere repetition.

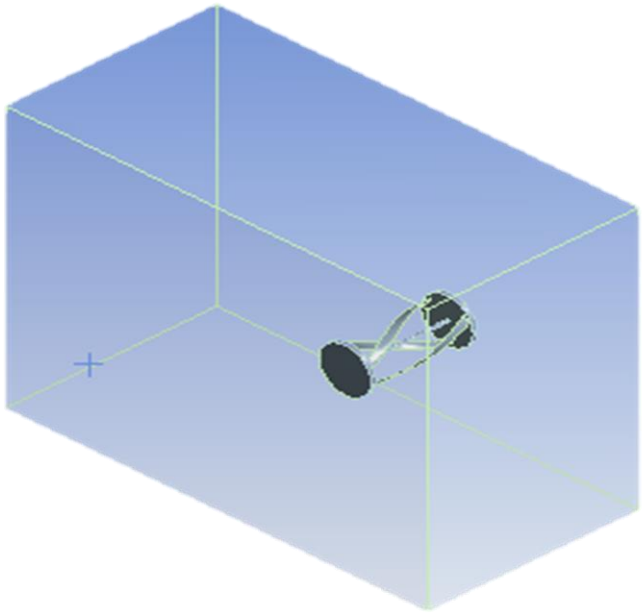

Figure 19-Domain model for CFD simulation

4.7. RESIDUAL VALUES

3D CFD Simulations were conducted to simulate the performance of the Water Turbine. For the input parameters, our simulations did converge to yield a negligible error output. In any CFD Simulation, ‘**Residual Values**’ give a measure of the local imbalance of each conserved variable. Every cell in the working domain will have some local imbalance associated with it at any moment in time and thus it will also have some Residual Value. To increase the credibility and precision of our solution we want the residual values to be of minimum value. These Residual values arise from the iterative solutions that govern the fluid domain under study.

For our CFD, the residual estimations turned out to be in the range of 10^{-3} to 10^{-5}. Such lower errors in our analysis prove the high quality of our results. The convergence of these residuals is further shown in the image below. This figure is for the residuals with elements of boundary size of 5 mm.

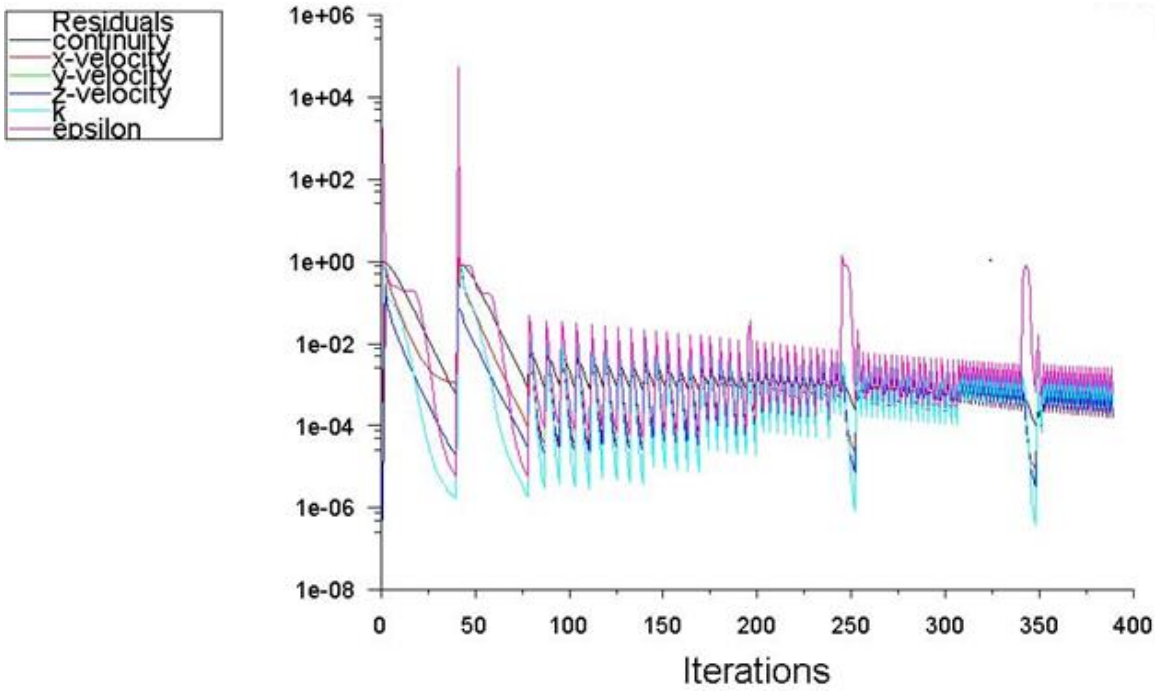

Figure 20-Residual Values for CFD Simulation

4.8. GRID INDEPENDENCE

Grid Independence is a term that refers to the process of making the analysis of our solution independent of mesh size. If the solution of CFD problem converges for a smaller mesh size but fails to converge at a larger mesh size then we conclude that our solution is dependent upon the mesh size and if we change the mesh size, we'll get a different result for our analysis.

For a solution to be Grid Independent the magnitude of residual error for a smaller and a larger mesh size should be at least 10^{-4}. Usually we do grid independence test by taking the mesh size to be 1.5 times the size of the original mesh. In order to get credible results,

we want our solution to only depend upon the boundary conditions and the physics utilized and not on the size of our mesh.

4.9. RESULTS AND DISCUSSION

The CFD Model allowed us to calculate the moments generated by the turbine. This was then used to calculate the power and coefficient using the formulas

$$P = \mathrm{T}\omega \tag{20}$$

$$C_p = \frac{\mathrm{T}\omega}{\frac{1}{2}\rho A U^3} \tag{21}$$

Table 5-Power and Coefficient of Performance calculation from moment values

Mesh No.	Moment (Nm)	Power (W)	Coefficient of Performance
1	3.95	57.67	0.37
2	3.83	55.983	0.35
3	3.83	55.983	0.345
4	3.7132	54.2886	0.341

The following diagrams show the pressure contour from the 5 mm CFD Analysis.

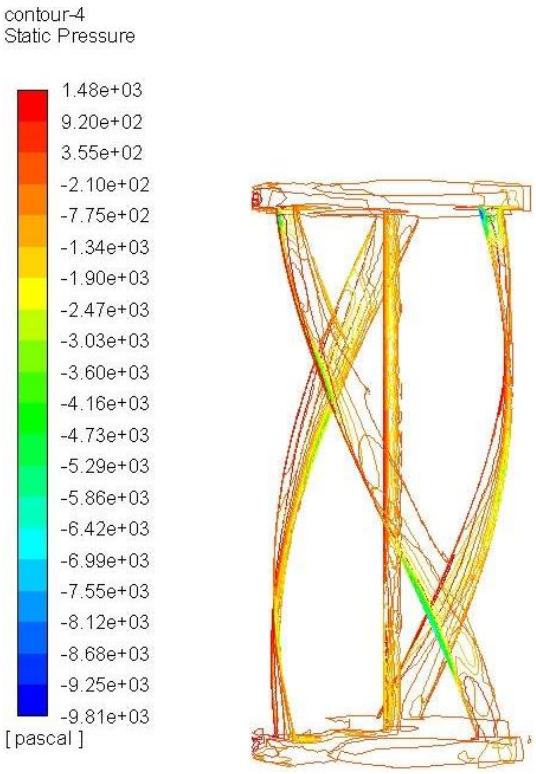

Figure 21-Pressure contour

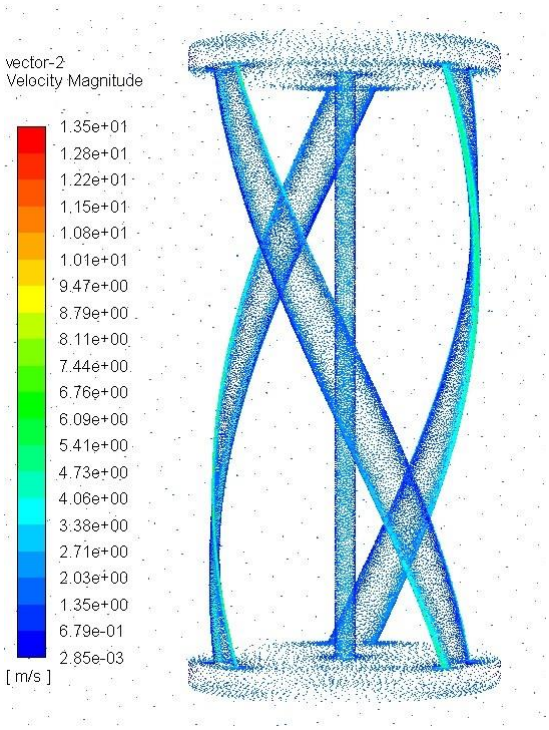

Figure 22-Velocity vectors

4.10. CONCLUSION

The final results are mentioned in the following table

Table 6-Result comparison: Analytical vs. CFD

	Power Output (W)	**Coefficient of Performance**
Q-Blade	48	0.32
CFD	54.2886	0.341

Our analysis for the turbine using both the techniques yielded similar results. This approves the quality of our analysis.

5. MANUFACTURING OF TURBINE ASSEMBLY

5.1. DESIGN PARAMETERS

Our target was to develop a turbine that would operate under low flow and low head conditions, and was capable of exploiting these conditions with a high self-starting ability. For this purpose, the lift based Darrieus turbine was selected due to its higher efficiency. Moreover, the helical profile of blades was adopted to attain better self-starting capability and minimized torque fluctuations.

After conducting various simulations in Q-Blade, it was agreed to design a 4-blade turbine with NACA 0018 Airfoil with chord length of 5.5 cm. The dimensions of turbine include height 0.38m, diameter 0.25m, Turbine Aspect Ratio of 1.52 and solidity of 0.29. This will produce a maximum torque of 4.3 Nm with power output of 63 W.

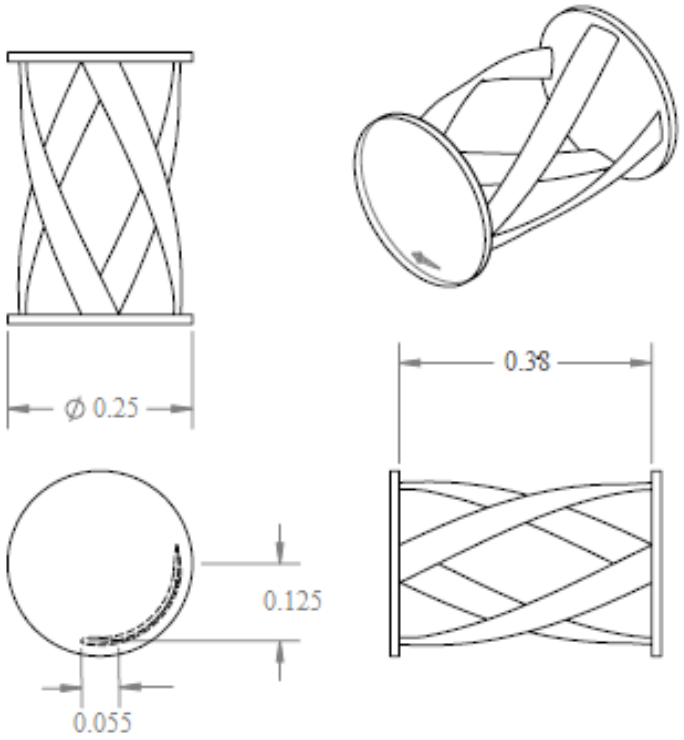

Figure 23-Final Dimensions of Turbine

.

5.2. BLADES FABRICATION TECHNIQUE

In order to ensure that the turbine would operate as per the desired analysis, it was mandatory for us to attain accurate hydrofoil shapes with minimum defects, along with the necessary higher strength-to-weight ratio. Three possibilities were considered as mentioned below, each with its pros and cons

5.2.1. 3D Printing

The most feasible and easy to manufacture option that we had was to get the whole turbine printed in one piece. However, the available sizes of the Printing beds were quite limited and required us to print the blades in two parts. Considering the fact that coupling the two parts of each would lead to a weaker joint, as well as would result in an imprecise and an inaccurate blade profile. Hence, this option was not considered.

5.2.2. Machining

The machining of aluminum blocks to develop blades meant we would be able to attain both the desired strength-to-weight ratio and highly accurate blade profile. This, however, was a very expensive option. Apart from the operating cost of machines, it required large blocks of aluminum for each blade, owing to its helical profile. Again, this option had to be eliminated.

5.2.3. Sand Casting

The third option was to get the blades casted. It required development of one blade pattern (wood or polymer), which would be used to cast the rest of the blades. Although investment casting promised more accuracy in the blade profile, sand casting seemed to be the most feasible one, considering our constrained budget. Moreover, this option yielded acceptable results in the former projects as well.

For material selection, a comparative analysis is presented in the following table. A score was given out of 5 for each category as per our desired requirements.

Table 7-Material selection matrix

Material	Strength	Weight	Finish	Price	TOTAL
Carbon fiber	5	5	5	1	16
6061 Aluminum	5	3	5	5	18
1018 Mild Steel	5	1	1	5	12

Based on the defined matrix, we opted for 6061 Aluminum.

5.3. FASTENING TECHNIQUE

An important part of the manufacturing phase was to decide the fastening mechanism that would be used to join the blades to the support. For this purpose, different options were considered. Among them, one was the use of bolts and nuts to join the blade with the support plate. The other option was to get the blade welded to another aluminum plate. The latter option was more practical due to its advantages in terms of its ***higher strength*** and ***reduced vibration***.

5.4. DETAILED MANUFACTURING PROCESURE

5.4.1. 3D Printing

In order to ensure maximum accuracy of the blade profile – the most important feature responsible for generation of desired lift forces for producing required torque and optimum power – it was decided to go for **3D printing** for developing molds for the helical-profile blades. The pattern was made into two symmetrical halves joined together video due to the limitation of the size of 3D Printing Bed. The following figure shows the two halves joined together, used as a pattern for sand casting.

Figure 24-3D Printed Blade Pattern

5.4.2. Sand Casting

After the development of the 3D pattern, the sand casting facility provided by DMRC at assembly was approached. The desired material, including 5 kg of Aluminum and 10 litres of motor oil, were provided. However, the quality of sand casting was unacceptable as the blades had a lot of pinholes and pits. The blades, circled in red, had to be filed by hand as shown in the figure below to improve dimensional accuracy.

Figure 25-Filing of Blades

Each blade, moreover, was casted into two pieces. Although we approached an Aluminum welder for joining the two pieces, the said approach did not yield an accurate profile. Hence, the casting procedure had to be repeated again, this time from a private vendor in Gawal Mandi, Rawalpindi.

5.4.3. Buffing

The image below shows the final blade that we attained after getting it polished and buffed from Kamran Market Saddar, Rawalpindi.

Figure 26-Grinding and Buffing of Blades

5.4.4. Welding

Aluminum welding offered a lot of advantages, but it required a detailed market survey before we execute this idea properly. Although referred by DMRC, the quality of the work of the approached vendor unfortunately did not meet the standard requirements. The following figures show the results after welding only the bottom plates with the plate. It can be seen that the blades were not welded at the accurate positions, and hence the second plate, if welded in the same position, would have resulted in a non-symmetrical profile. This has been highlighted by the red circles as shown in the picture below.

Figure 27-Manufacturing Defects

The blades were carefully separated from the plate. These were then grinded, polished and buffed before they were taken to the aluminum welder. This time, we approached Shireen Welders in Saddar, Rawalpindi, who carefully welded the blades as desired. The final picture of the main part of the turbine assembly is shown below.

Figure 28-Turbine Rotor

5.4.5. Support Design

In order to the aforementioned on the shaft, a support mechanism was designed in SolidWorks. As shown in the photo below, chucks were manufactured using lathe machine out of polished steel to fasten the plates with the steel shaft.

Figure 29-Support Collar

5.4.6. Balancing

In order to ensure smooth operation, static balancing was conducted. Dynamic balancing was not considered since the turbine was to operate at lower RPMs. Holes were drilled on the plates at the appropriate positions to achieve the requirement.

Figure 30-Static Balancing Assembly

6. INSTRUMENTATION DEVELOPMENT

6.1. NOVELTY: PERFORMANCE ANALYSIS METHODOLOGY

Our aim in this Final Year Project is to develop a reliable mechanism that would be able to yield **quantifiable output** of our proposed turbine assembly.

For this purpose, two major options were considered.

6.1.1. Incorporation of an Electrical System

A possibility was to couple power turbine with either a generator, a permanent magnet DC motor, or an alternator. All these options, however, were rejected because they would operate on a power range much higher than the predicted output of our turbine. Moreover, the said components were also expensive. Most importantly, it was realized that the handling of these electrical components would be really difficult, especially in flowing water inside the canals.

6.1.2. Development of a Mechanical System

Considering the weaknesses of the electrical systems, it was necessary for us to develop a mechanical system that would be able to generate reliable torque and power data. Drawing inspiration from the Pelton turbine assembly, we decided to design a rope and pulley dynamometer that would be suited specifically for our turbine.

The proposed system helps us to measure the brake torque at different RPM in different test locations. For each test location, different readings of forces were recorded and hence the torque and power were recorded at respective RPMs. This method is covered in detail in the Data Analysis section.

6.2. INSTRUMENTATION TIMELINE

This section describes the important tasks that were conducted in order to develop a successful Rope and Pulley dynamometer. These include the development of strong support, a tailored rope, customized pulleys, a force meter, newton weights and other accessories.

6.2.1. Light Weight Pulleys

Pulleys are an integral part of the dynamometer. Lightweight pulleys were required in order to ensure that the external system had the lowest possible value of the moment of inertia. Hence, instead of opting for the easily available steel pulleys, we decided to purchase Teflon pulleys. These were later altered by adding polished steel bushings in order to pin them to the steel shaft.

The following image shows the pulleys before and after the bushings were inserted. The figure also shows the connecting iron parts that were used to join one of these pulleys with the frame.

Figure 31-Teflon Pulleys

6.2.2. Tailored Rope

The following figure shows strong nylon rope that was selected to withstand the greater external load to be applied on the dynamometer. Clips were sewed at both the ends in order to support the force meter as well as the additional load to be applied using hanger.

Figure 32-Purpose-built Rope

6.2.3. Strong Support

A strong support was essential in order to support the large tensile load that would be applied by the rotating turbine assembly. Various configurations and different gauge steel sheets were considered before making the final decision.

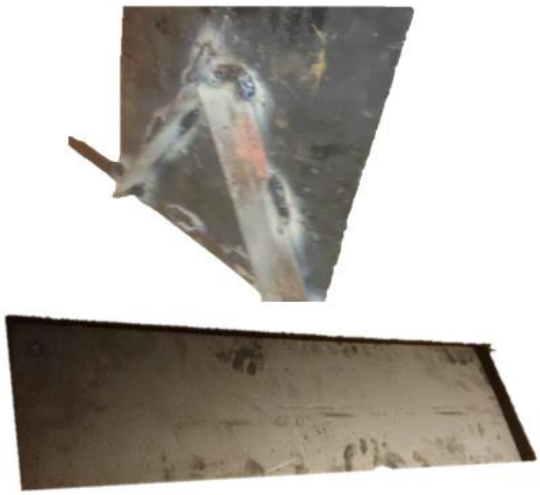

Figure 33-Support for Rope Pulley Dynamometer Assembly

6.2.4. Force Meter

A digital weighing scale, with accuracy up to 3 decimal places, was purchased from Bilal Traders, PWD Market in Islamabad. The price of this balance was Rs. 400.

Figure 34-Digital Force Meter

6.2.5. Weights

It was agreed to add known weights at one end of the rope. The net force would then be used to calculate the torque being produced by the turbine at a certain RPM. These were issued from Dynamics and Controls Lab, SMME.

Figure 35-Weights and Hanger

6.2.6. Bearing Selection

Bearing plays a vital role in the turbine assembly. The selection of bearing depends on the type of forces acting on the shaft and operating conditions for the bearing. The turbine experiences radial forces due to its spinning motion as well as the thrust force produced by flowing water, whereas it undergoes axial loading due to the weight of turbine assembly, comprising of turbine shaft, blades, alternator, pulley system and bearings.

For the turbine, the axial forces present are smaller than radial forces since the weight of the overall Turbine assembly is much lower than force exerted by the water flow. Moreover, the bearing would be operating inside the water; this meant the bearing also needed to possess water proof characteristics. Hence **NTN UCP 202 DDU Ball Bearing** was an optimum choice for this part. The DD identifies double seal which means the bearing is **water proof**.

The bearings were purchased from Khurram Bearing City Saddar, Rawalpindi. Each bearing was of Rs. 750. The bearing housings were also purchased from the same vendor, with each costing Rs. 600. The bearing fitted inside the housing can be seen in the following figure.

Figure 36-UCP 202 Bearing

6.2.7. Shaft Design

The material selection and calculations for the shaft design are mentioned. The final parameters are mentioned in table below

Table 8-Shaft parameters

Shaft Design	
Material	AISI 304 SS
Height	4 ft.
Diameter	9/16 inch

6.2.8. Turbine Central Shaft Calculation

This has been calculated assumed flow velocity of 2 ms^{-1}.

The RPM of turbine is given by

$$N = \frac{TSR \times U \times 60}{\pi D} \quad \textbf{(22)}$$

Where

TSR = 2

U = 2 ms^{-1}

D = 0.25 m

Hence, N = 280

The area of turbine is given by

$$A_{frontal} = A_{blades} + A_{shaft} \quad \textbf{(23)}$$

Where

A_{blades} = no. of blades x height x chord length

= 4 x 0.38 x 0.055

= 0.0836 m^2

A_{shaft} = height x diameter

= 0.38 x 0.25

= 0.095 m^2

Hence $A_{frontal}$ is 0.1786 m^2.

The thrust force F by the water can be calculated as

$$F = \frac{1}{2} C \rho A_{frontal} U^2 \quad \textbf{(24)}$$

Where

F = Thrust Force by water

C = Coefficient of Thrust; 0.9 for this turbine

ρ = Density of fluid; 1000 kgm^{-3} for water

$A_{frontal}$ = 0.1786 m^2

This yields F to be 320 N.

The torque is given by

$$T = \frac{P \times 60}{2\pi \times N} \quad \textbf{(25)}$$

Where

P = 40 W

N = 280

The torque T comes out to be 2.38 Nm.

The maximum bending force is possible at the center of shaft, assuming bearings provide support, is calculated as:

M = F x R

= 320 x (0.25/2)

= 40 Nm

The total weight of turbine assembly (including shaft and accessories) is assumed to be 3.5 kg. This gives the weight W as follows:

W = m x g

= 3.5 x 9.81

= 34.335 N

Now, the forces and moments acting on the turbine are depicted in the image below:

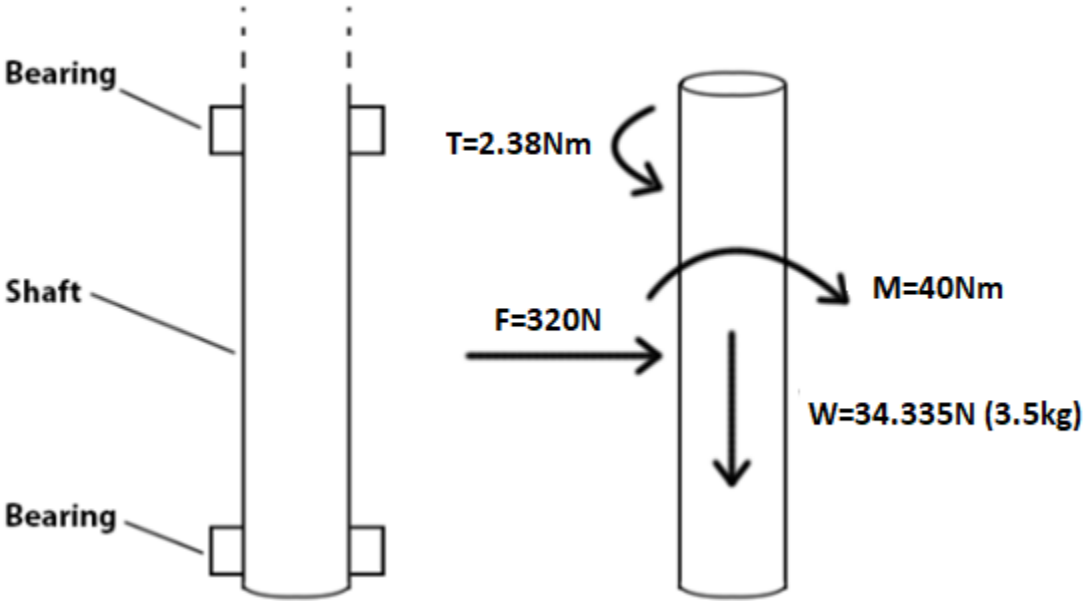

Figure 37-Consolidated Forces and Moments on Shaft

These dynamic components contribute into the production of normal and shear stresses. These are represented by the diagram below:

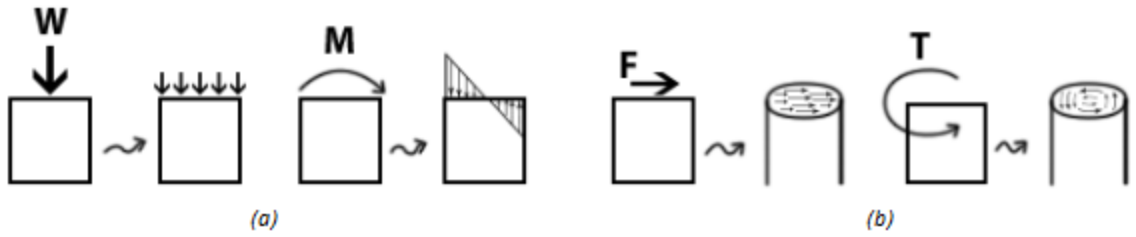

Figure 38-Force Distribution on Shaft

Let us assume a shaft with the following geometric properties.

Table 9-Shaft material properties

Material Properties AISI 304 SS	
Yield Strength (MPa)	215
Tensile Strength (MPa)	505
Diameter (D)	0.050
Radius (c)	0.025
Height (h)	1.125
Area (A)	0.00196345
Bending Moment of Inertia (I)	3.068e-7
Polar Moment of Inertia (F)	6.136e-7

The maximum possible Von Mises stress possible on the shaft would be when all these forces are acting at a certain element on the shaft

$$\sigma_{normal,max} = \frac{W}{A} + \frac{Mc}{I} \quad \textbf{(26)}$$

$$\sigma_{shear,max} = \frac{Tc}{J} + \frac{4F}{3A} \quad \textbf{(27)}$$

And

$$\sigma_{\text{von mises,max}} = \sqrt{\sigma_{\text{normal,max}}{}^2 + \sigma_{\text{shear,max}}{}^2} \quad \textbf{(28)}$$

From calculations using the values above, we get:

$\sigma_{\text{normal,max}} = 11.75$ MPa

$\sigma_{\text{shear,max}} = 0.329$ MPa

$\sigma_{\text{von mises,max}} = 11.77$ MPa

Since the maximum stress on the shaft is much lower than the Yield Strength for the shaft, the proposed design is safe and viable to use.

6.3. FINAL ASSEMBLY

The following figure shows the final turbine assembly. The novelty resides in the design of the low cost torque measurement system of the developed prototype, encircled in red.

Figure 39-Prototype Assembly

7. RESULTS AND DISCUSSIONS

7.1. TEST SITE

Testing of the turbine was carried out in April 2019 in the daughter canal of Khanpur Dam near UET Taxila. The experiment was conducted at four separate locations along the length of the water channel to maximize the sample size. Moreover, due to a large safety factor we were able to test the turbine above design conditions. This is evident from the following images.

Figure 40-Turbine under operation (unloaded)

Figure 41-Turbine under operation (loaded)

The results culminated in better generalizations for the analytical and practical assumptions. The coordinates of the locations are given as follows

- Experiment 1 – 33.779854, 72.818686
- Experiment 2 – 33.780132, 72.817806
- Experiment 3 – 33.779901, 72.815878
- Experiment 4 – 33.782213, 72.791198

7.2. PERFORMANCE CURVES

The performance curves were plotted from the experimental data illustrated in Appendix 1. The relationships quantified through graphs are listed as follows

- Torque vs. RPM
- Power vs. RPM

The data for the required curves was obtained by mechanically loading the turbine up to the stall condition to obtain its maximum performance criterion under specific testing conditions. The flow speeds were obtained by measuring the dynamic head of the channel at different locations. The trend obtained is in agreement with the established norm for characteristic curves of a turbine.

At low RPMs, the product in accordance with the aforementioned equation is low which ultimately results in a low value of power. At higher RPMs, the turbine creates a phenomenon known as the **"Wall Effect"**. As a result the water goes around the turbine instead of going through it thereby effectively decreasing the lift force generating torque. A lower torque again leads to lower power in accordance with the above relation. The curves are given below.

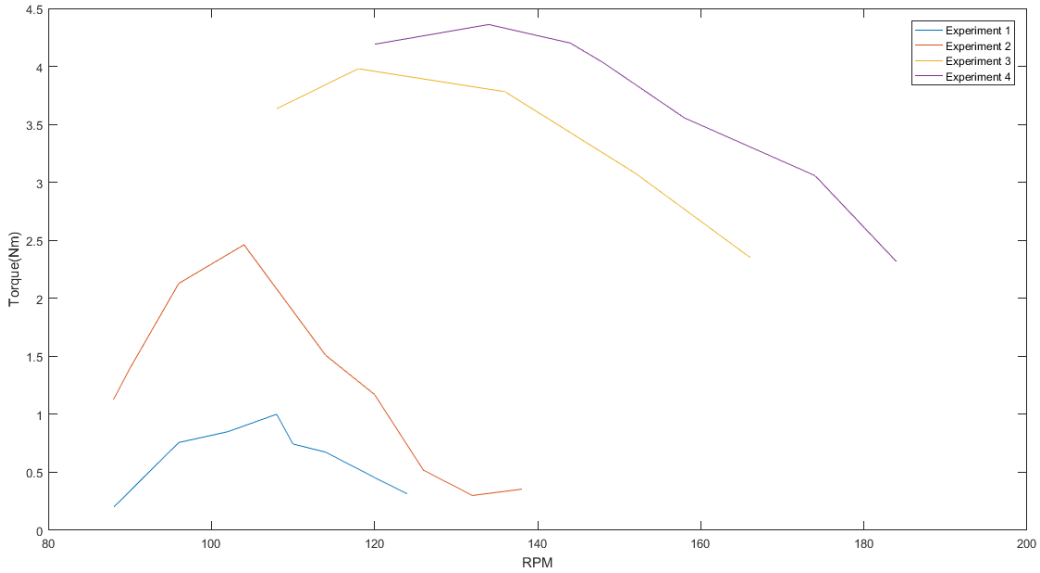

Figure 42-Torque vs RPM Curve

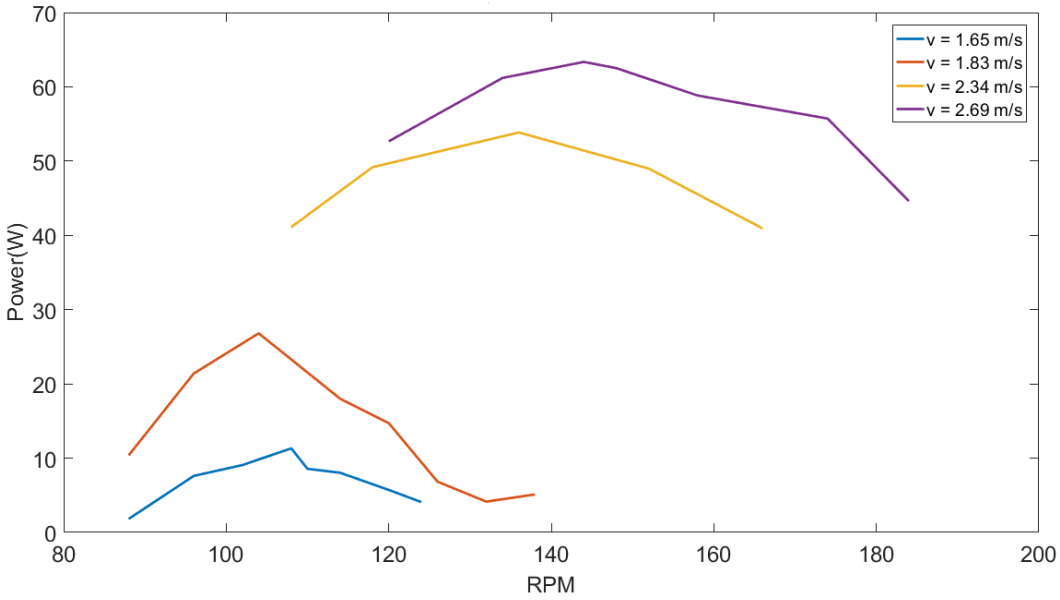

Figure 43-Power vs RPM Curve

7.3. RESULTS VERIFICATION

The comparison of theoretical and actual results is shown below. The obtained values of power are in close proximity to predicted values however, the error increases as the flow speed increases. This can be attributed to the phenomenon of flow separation which becomes pronounced at higher speeds. As a result, our choice of four blades instead of three is more severely affected by the extreme conditions. Furthermore, turbulence is induced by the hindrance offered by the stand despite its large size. Consequently the wake region of each blade grows bigger ultimately affecting the performance of approaching blades and hence the complete turbine rotor. A slight disparity in established trend can be attributed to human error in observation.

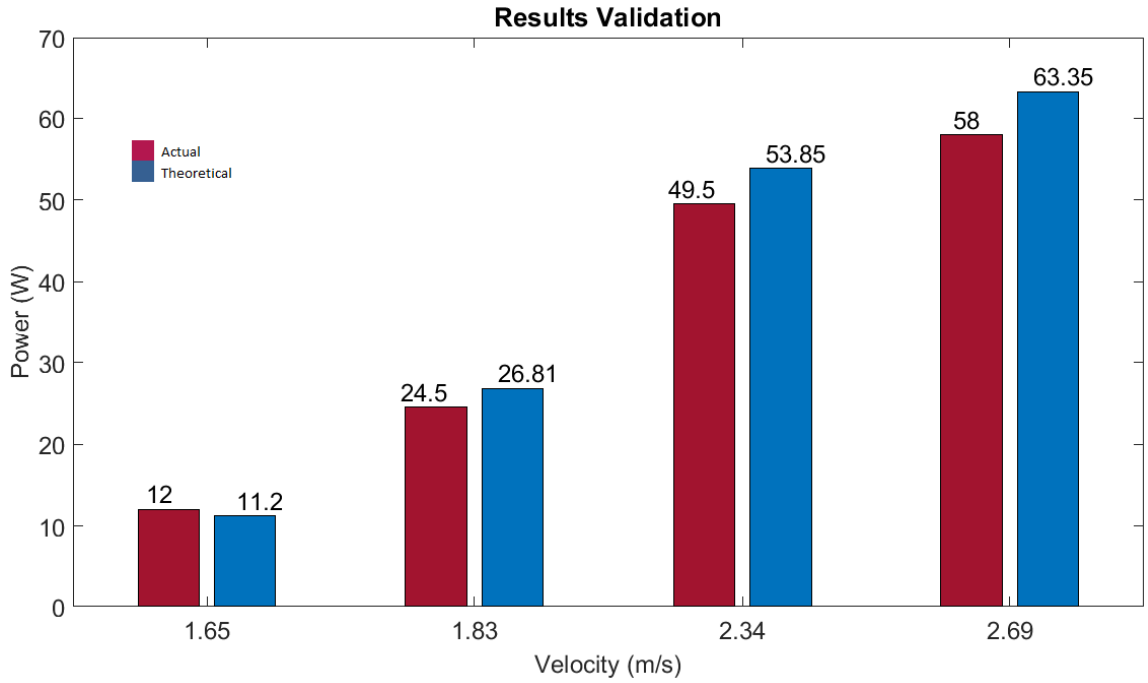

Figure 44-Performance Comparison

7.4. ERROR ANALYSIS

RANGE CALCULATION

Maximum frames per second

For accurate data acquisition

Maximum allowable degrees of revolution per frame

$$360^o$$

Degrees of revolution per second

$$360 * 30 = 10800^o$$

Revolutions per second

$$\frac{10800}{360} = 30$$

RPM

$$30 * 60 = 1800$$

This is the upper limit of this measurement technique

ERROR IN MEASUREMENT

Maximum speed of rotation

$$212rpm$$

Revolutions per second

$$\frac{212}{60} = 3.53$$

Degrees of revolution

$$3.53 * 360 = 1270.8^o$$

Degrees of revolution per frame

$$\frac{1270.8}{30} = 42.3^o$$

Uncertainty in capturing one revolution

$$(42.3 * 9) - 360 = 20.7^o$$

For maximum speed, error in measurement

$$\pm 12.19 rpm$$

ERROR IN POWER MEASUREMENT

$$P = \mathrm{T}\omega$$

$$P = (m_2 - m_1) * g * R * \frac{2\pi N}{60} \quad \textbf{(29)}$$

$$\frac{\delta P}{P} = \frac{\delta w}{w} + \frac{\delta R}{R} + \frac{\delta N}{N} \quad \textbf{(30)}$$

$$\delta P = \left(\frac{0.005}{w} + \frac{1}{39.4} + \frac{12.19}{N}\right) * P \quad \textbf{(31)}$$

The error in each case is

$$\delta P_1 = 1.6085W$$
$$\delta P_2 = 3.8931W$$
$$\delta P_3 = 6.3527W$$
$$\delta P_4 = 7.1371W$$

8. CONCLUSION

The purpose of this study was to determine the technical and economic feasibility of a Gorlov helical Turbine. A vigorous study that included analytical and numerical approaches was conducted. The findings are listed as follows

- The efficiency of the turbine is limited by the Betz Limit [19] which states that no turbine can capture more than 59.3% of the kinetic energy in a Newtonian fluid. The efficiency of the turbine came out to be 0.25 in our case which is consistent with other research work and observations.
- A four bladed turbine is better than a two bladed design on account of design integrity and imbalance in operation. A higher blade wrap also provides significant challenges.
- A three bladed design is superior to a four bladed design and greater due to increased surface drag as the number of blades increase. This has also been observed first hand through simulations.
- A higher aspect ratio leads to better overall performance while increase in the solidity results in a dip in performance. However, higher values of solidity will aid the self-starting of turbine under less favorable conditions. The values of solidity and aspect ratio can be used to non-dimensionalized the turbine design. Chosen values were 0.29 and 1.52 respectively.
- A larger radius will result in more power generation due to increased torque. However, fluid velocities play a more important role since power is expressed as the function of the cube of the free stream velocity. The speed under test conditions ranged from $1.65ms^{-1}$ to $2.7ms^{-1}$.
- Q-Blade under predicts the final result. However, that is in accordance with the literature review [20].

Renewable energy installations have improved in efficiency over the years. Climate change is real and the idea of generating power through environment conservation and ensuring a sustainable operation is gaining traction every day.

Global installed generation capacity is 2.2 TW [21]. This system could be implemented in Pakistan through these small-scale machines, especially in northern remote areas to connect them to the national grid so they can contribute to the development and welfare of their families and eventually the whole region.

8.1. FUTURE RECOMMENDATIONS

Cambered profile was selected for the original turbine design with the intention of reducing starting torque application problem. That theory still needs to be tested in real time situation.

NACA profiles of only 4 digits were used. However, 5 or 6 digit profiles can be tested for research purposes since academic data is not in much abundance and it will give us new perspective as to possibilities attached with those profiles.

Helical angle allows for the rotation of the blades from any direction of water. However, the turbine was erected vertically and was tested in the same orientation in the canal. Testing it with varying orientations will also open new dimension of understanding the functioning of the turbine.

The scope of improvement beyond this project includes

- Development of specific analytical model for helical blade design in the hydrokinetic domain
- Exploring the potential of tidal power since the energy reserves are much greater than canals. The exploitable energy in shallow areas is about 120GW [22].

9. REFERENCES

[1] J. C.- science and undefined 2003, "Human population: the next half century," *science.sciencemag.org*.

[2] B. Güneralp, Y. Zhou, … D. Ü.-V.-P. of the, and undefined 2017, "Global scenarios of urban density and its impacts on building energy use through 2050," *Natl. Acad Sci.*

[3] "| Ministry of Finance | Government of Pakistan |." [Online]. Available: http://www.finance.gov.pk/survey_1718.html. [Accessed: 28-Jan-2019].

[4] M. Hassan, M. K. Afridi, and M. I. Khan, "An overview of alternative and renewable energy governance, barriers, and opportunities in Pakistan," *Energy Environ.*, vol. 29, no. 2, pp. 184–203, Mar. 2018.

[5] "Energy Efficiency." [Online]. Available: http://www.ren21.net/gsr-2018/chapters/chapter_07/chapter_07/. [Accessed: 28-Jan-2019].

[6] O. Ellabban, H. Abu-Rub, F. B.-R. and S. Energy, and undefined 2014, "Renewable energy resources: Current status, future prospects and their enabling technology," *Elsevier*.

[7] F. Qureshi, B. A.-11th I. C. A. C. Eng, and undefined 2014, "Hydropower potential in Pakistan," *researchgate.net*.

[8] M. Khan, G. Bhuyan, M. Iqbal, J. Q.-A. energy, and undefined 2009, "Hydrokinetic energy conversion systems and assessment of horizontal and vertical axis turbines for river and tidal applications: A technology status review," *Elsevier*.

[9] P. A.-R. E. T. and Sustainable and undefined 2005, "Challenges for the promotion of renewable-energy technologies in Pakistan," *climateinfo.pk*.

[10] "Types of Hydropower Turbines | Department of Energy." [Online]. Available: https://www.energy.gov/eere/water/types-hydropower-turbines. [Accessed: 28-Jan-2019].

[11] L. Schwartz and W. Wilson, "Case studies of the legal and institutional obstacles and incentives to the development of small-scale hydroelectric power. Executive summary," 1979.

[12] B. Yang, X. S.-O. Engineering, and undefined 2012, "Hydrofoil optimization and experimental validation in helical vertical axis turbine for power generation from marine current," *Elsevier*.

[13] M. Alam, M. I.-E. and C. Engineering, undefined 2009, and undefined 2009, "Design and development of hybrid vertical axis turbine," *ieeexplore.ieee.org*.

[14] J. Manwell, J. McGowan, and A. Rogers, *Wind energy explained: theory, design and application*. 2010.

[15] M. M.- Energy and undefined 2012, "Performance investigation of H-rotor Darrieus turbine with new airfoil shapes," *Elsevier*.

[16] L. Voigt, "Comparison of turbulence models for numerical calculation of airflow in an annex 20 room," 2000.

[17] H. Schlichting and K. Gersten, *Boundary-layer theory*. 2016.

[18] A. Alaimo, A. Esposito, A. Messineo, C. O.- Energies, and undefined 2015, "3D CFD analysis of a vertical axis wind turbine," *mdpi.com*.

[19] A. Betz, "Introduction to the theory of flow machines. extend to both, and laying cable requires extensive(DG Randall, Trans.) Oxford," 1966.

[20] P. Bachant, M. W.- ASME-JSME, and undefined 2011, "Experimental investigation of helical cross-flow axis hydrokinetic turbines, including effects of waves and turbulence," ... *.asmedigitalcollection.asme.org*.

[21] H. L.- Energy and undefined 2007, "Renewable energy strategies for sustainable development," *Elsevier*.

[22] A. Niblick, "Experimental and analytical study of helical cross-flow turbines for a tidal micropower generation system," 2012.

APPENDIX 1: DATA ACQUISION

The experimental has been recorded in tabular form. The test matrices are given as follows.

Table 10-Test Matrix for Experiment 1

U = 1.65 m/s								
RPM	124	120	114	110	108	102	96	88
Rotational Velocity (rad/s)	12.9852	12.5664	11.9381	11.5192	11.3097	10.6814	10.0531	9.2153
Reading on Balance (kg)	0.395	0.635	0.895	1.015	1.285	1.45	1.63	1.69
Tension (N)	3.875	6.2294	8.78	9.9572	12.6059	14.2245	15.9903	16.5789
Added Weights (N)	2	4	6	7	9	11	13	15
Slack (N)	3.0791	5.0791	7.0791	8.0791	10.0791	12.0791	14.0791	16.0791
Net Force (N)	0.7959	1.1502	1.7009	1.8781	2.5267	2.1454	1.9112	0.4998
Torque (Nm)	0.3152	0.4555	0.6735	0.7437	1.0006	0.8496	0.7568	0.1979
Power (W)	4.0924	5.724	8.0407	8.5669	11.316	9.0747	7.6085	1.8239

Table 11-Test Matrix for Experiment 2

U = 1.83 m/s								
RPM	138	132	126	120	114	104	96	90
Rotational Velocity (rad/s)	14.4513	13.823	13.1947	12.5664	11.9381	10.8909	10.0531	9.4248
Reading on Balance (kg)	0.405	0.595	0.855	1.125	1.416	1.865	2.085	2.1
Tension (N)	3.9731	5.8369	8.3876	11.0363	13.891	18.2957	20.4538	20.601
Added Weights (N)	2	4	6	7	9	11	14	16
Slack (N)	3.0791	5.0791	7.0791	8.0791	10.0791	12.0791	15.0791	17.0791
Net Force (N)	0.894	0.7578	1.3085	2.9572	3.8119	6.2166	5.3747	3.5219
Torque (Nm)	0.354	0.3001	0.5181	1.171	1.5095	2.4618	2.1284	1.3947
Power (W)	5.1158	4.1484	6.8368	14.7156	18.0204	26.8106	21.397	13.1445

Table 12-Test Matrix for Experiment 3

U = 2.34 m/s					
RPM	166	152	136	118	108
Rotational Velocity (rad/s)	17.3835	15.9174	14.2419	12.3569	11.3097
Reading on Balance (kg)	0.92	1.31	1.695	1.95	2.065
Tension (N)	9.0252	12.8511	16.628	19.1295	20.2577
Added Weights (N)	2	4	6	8	10
Slack (N)	3.0791	5.0791	7.0791	9.0791	11.0791
Net Force (N)	5.9461	7.772	9.5489	10.0504	9.1786
Torque (Nm)	2.3547	3.0777	3.7813	3.98	3.6347
Power (W)	40.9321	48.9892	53.8535	49.1801	41.1076

Table 13-Test Matrix for Experiment 4

	U = 2.69 m/s						
RPM	184	174	158	148	144	134	120
Rotational Velocity (rad/s)	19.2684	18.2212	16.5457	15.4985	15.0796	14.0324	12.5664
Reading on Balance (kg)	0.91	1.305	1.535	1.76	1.905	2.15	2.31
Tension (N)	8.9271	12.802	15.0584	17.2656	18.6881	21.0915	22.6611
Added Weights (N)	2	4	5	6	7	9	11
Slack (N)	3.0791	5.0791	6.0791	7.0791	8.0791	10.0791	12.0791
Net Force (N)	5.848	7.7229	8.9793	10.1865	10.609	11.0124	10.582
Torque (Nm)	2.3158	3.0583	3.5558	4.0339	4.2011	4.3609	4.1905
Power (W)	44.622	55.7258	58.833	62.5188	63.3518	61.1942	52.659

APPENDIX 2: MATLAB CODE FOR PERFORMANCE CURVES

The following MATLAB code is used to generate the torque and power curves.

```
------------------------- Experiment no. 1 --------------------------

coordinates = [33.7626, 72.8328];
head = 0.14; velocity = 1.65; rpm_unloaded = 144;
rpm1 = [124 120 114 110 108 102 96 88]; omega1 = rpm1 * 2 * pi / 60
force_meter1 = [0.395 0.635 0.895 1.015 1.285 1.450 1.630 1.690];
force_tension1 = 9.81 * force_meter1
force_weights1 = [2 4 6 7 9 11 13 15];
force_slack1 = 0.11*9.81 + force_weights1
force_net1 = force_tension1 - force_slack1

torque1 = force_net1 * 0.396
power1 = times(torque1,omega1)
------------------------- Experiment no. 2 --------------------------

coordinates = [33.7626, 72.8328];
head = 0.17; velocity = 1.83; rpm_unloaded = 156;
```

```
rpm2 = [138 132 126 120 114 104 96 90 88]
omega2 = rpm2 * 2 * pi / 60

force_meter2 = [0.405 0.595 0.855 1.125 1.416 1.865 2.085 2.100 2.235]
force_tension2 = 9.81 * force_meter2
force_weights2 = [2 4 6 7 9 11 14 16 18];
force_slack2 = 0.11*9.81 + force_weights2
force_net2 = force_tension2 - force_slack2

torque2 = force_net2 * 0.396
power2 = times(torque2,omega2)


-------------------------- Experiment no. 3 ---------------------------


coordinates = [33.7620, 72.8522];
head = 0.28 ; velocity = 2.34; rpm_unloaded = 180;

rpm3 = [166 152 136 118 108]
omega3 = rpm3 * 2 * pi / 60

force_meter3 = [0.920 1.310 1.695 1.950, 2.065]
force_tension3 = 9.81 * force_meter3
force_weights3 = [2 4 6 8 10]
force_slack3 = 0.11*9.81 + force_weights3
force_net3 = force_tension3 - force_slack3

torque3 = force_net3 * 0.396
power3 = times(torque3,omega3)

-------------------------- Experiment no. 4 ---------------------------

coordinates = [33.7620, 72.8522];
head = 0.37; velocity = 2.69; rpm_unloaded = 212;
```

```
rpm4 = [184 174 158 148 144 134 120]
omega4 = rpm4 * 2 * pi / 60
force_meter4 = [0.910 1.305 1.535 1.760 1.905 2.150 2.310];
force_tension4 = 9.81 * force_meter4
force_weights4 = [2 4 5 6 7 9 11];
force_slack4 = 0.11*9.81 + force_weights4
force_net4 = force_tension4 - force_slack4

torque4 = force_net4 * 0.396
power4 = times(torque4,omega4)

------------------------------- Graphs ------------------------------

figure; plot(rpm1, torque1,'LineWidth',2); hold on; plot(rpm2,
torque2,'LineWidth',2);
plot(rpm3, torque3,'LineWidth',2); plot(rpm4, torque4,'LineWidth',2);
hold off;
set(gca,'FontSize',18);
title({'Torque vs RPM curve'},'FontSize',20);
legend ({'v = 1.65 m/s', 'v = 1.83 m/s', 'v = 2.34 m/s', 'v = 2.69
m/s'},'FontSize',14);
xlabel('RPM','FontSize',18); ylabel('Torque(Nm)','FontSize',18);

figure; plot(rpm1, power1,'LineWidth',2); hold on; plot(rpm2,
power2,'LineWidth',2);
plot(rpm3, power3,'LineWidth',2); plot(rpm4, power4,'LineWidth',2);
hold off; set(gca,'FontSize',18);
title({'Power vs RPM curve'},'FontSize',20);
legend ({'v = 1.65 m/s', 'v = 1.83 m/s', 'v = 2.34 m/s', 'v = 2.69
m/s'},'FontSize',14);
xlabel('RPM','FontSize',18); ylabel('Power(W)','FontSize',18);
```